Stanford Geothermal Program
Interdisciplinary Research in
Engineering and Earth Sciences
STANFORD UNIVERSITY
Stanford, California

SGP-TR-63

RADON EMANATION MECHANISM FROM FINELY GROUND ROCKS

By

Kazuichi Satomi
Paul Kruger

October 1982

Financial support was provided through the Stanford Geothermal Program under Department of Energy Contract No. DE-AT03-80SF11459 and by the Department of Civil Engineering, Stanford University.

ACKNOWLEDGMENTS

The authors acknowledge with thanks the help and advice given by Lewis Semprini throughout this study. Thanks are due to Dr. Shigenori Maruyama of the Geology Department for his assistance with the petrographic observations of rock samples and to Luis Macias-Chapa for his fruitful suggestions.

This study was conducted with support of Kazuichi Satomi in obtaining his Degree of Engineer by the Nippon Steel Corporation. This report is adapted from Kazuichi Satomi's thesis.

TABLE OF CONTENTS

Acknowledgments ii

Abstract v

CHAPTER

1 INTRODUCTION 1

1.1 Radon as a Geothermal Reservoir Tracer 1

1.2 Objective of This Study 2

1.3 Scope of the Study 3

2 THEORY AND PREVIOUS STUDIES 5

2.1 Review of Previous Studies 5

2.2 Radon Characteristics 6

2.2.1 Radioactive decay of uranium series 6
2.2.2 Physical and chemical properties 11

2.3 Theory of the Emanation Process 12

2.3.1 Emanation power due to recoil 12
2.3.2 Emanation power due to diffusion 15
2.3.3 Overall emanation power 18
2.3.4 Buildup of emanation power 18
2.3.5 Temperature dependence of emanation power . . 19
2.3.6 Pressure effect of emanation power 20
2.3.7 Rock size effect on emanation power 21
2.3.8 Annealing effect of emanation power 22
2.2.9 Pore-fluid dependence on emanation power . . . 22

3 EXPERIMENTAL METHODS 24

3.1 Preparation of Rocks 24

3.1.1 Crushing and sieving 24
3.1.2 Baking and annealing 27

3.2 Rock Properties 27

3.3 Microscopic Observation 28

3.4 Experimental Procedures 28

3.4.1 Cold runs 28
3.4.2 Elevated-temperature runs 29

CHAPTER

3

3.5 Radon Extraction 32

3.5.1 Cold runs 32
3.5.2 Elevated-temperature runs 32

3.6 Radon Measurement 34

3.7 Radium Analysis 35

3.8 Measurement Statistics 35

3.8.1 Distribution of sample means 35
3.8.2 Sample variance 36

4 **RESULTS** 38

4.1 Room-Temperature Data 38

4.1.1 Annealing tests 38
4.1.2 Rock size tests 39

4.2 Elevated-Temperature Data 40

4.2.1 Radon buildup tests 40
4.2.2 Moisture tests 42

4.3 Microscopic Observations 44

4.4 Radium Analysis 44

5 DISCUSSION OF RESULTS 46

5.1 Annealing Effect 46
5.1.1 Change of emanation power in annealing tests . 46
5.1.2 Radium source in the graywacke sandstone . . . 48

5.2 Rock Size Effect 50
5.2.1 Change of emanation power 50
5.2.2 Segregation of minerals 52

5.3 Diffusion Process 53
5.3.1 Diffusion coefficient of radon 53
5.3.2 Time dependence of emanation power **59**
5.3.3 Moisture effect on emanation power **59**
5.3.4 Model of radon emanation mechanism from porous rock 63

6 CONCLUSION AND RECOMMENDATIONS 64

6.1 Conclusions 64

6.1.1 Major effects 64
6.1.2 Radon emanation mechanisms 65

6.2 Recommendations **65**

REFERENCES 66

ABSTRACT

Radon emanation from porous graywacke sandstone rock particles was measured under various reservoir conditions. Experiments were carried out to observe the dependence of emanation power on effects of annealing, rock size, and moisture content. The data were analyzed to determine the relative importance of recoil and diffusion processes for radon emanation from porous rock particles.

The annealing effect, associated with curing of crystal imperfections in a rock matrix, was quite small for the graywacke sandstone. The moisture effect, associated with water adsorbed on the rock pore surface, was much more pronounced. The magnitude of the effect was calculated from the results of emanation measurements under wet and dry conditions in the test reservoirs.

The effect of rock size was quite pronounced for small particle sizes. Emanation power from particles of diameters less than 300 μm showed steep increases with decreasing diameter. The dependence was inversely proportional, a function of $d^{1.5}$ for water and $d^{1.0}$ for nitrogen. Radon emanation from particle sizes larger than 300 μm in diameter showed less dependence on rock size. The effect is attributed to increases in surface area between particle and grain sizes created during crushing. The data are not sufficiently clear to show a specific relationship based on grain size.

The data from the moisture tests indicated that water adsorbed on the rock pore surface could account for much of the radon emanation. Emanation power increased rapidly with increased addition of water vapor to the rock samples to a vapor pressure of *40%* of the saturation vapor pressure. This value may correspond to the minimum thickness of a water layer on the rock surface which can absorb the kinetic energy of recoil radon atoms and stop them in the pore space. In the absence of adsorbed pore water, recoil radon atoms can penetrate into neighboring grains without contributing to the emanation power.

Diffusion coefficients were calculated from the experimental data and from a mathematical model. The agreement was satisfactory. Calculated values were of the order of 10^{-10} to 10^{-11} cm^2/sec for dry samples. The effects of moisture on diffusion could not be accounted for, and the diffusion coefficients calculated under wet conditions were about ten times larger, ranging from 10^{-9} to 10^{-10} to cm^2/sec.

A conceptual model of the emanation power in porous rock particles, where the granular pore surface area is large compared to the particle surface area indicates that direct recoil to the pore space should be the most important process.

CHAPTER 1

INTRODUCTION

1.1 RADON AS A GEOTHERMAL RESERVOIR TRACER

Radon is a useful in-situ tracer in geothermal reservoirs. Its occurrence and application in subsurface resources has been extensively reported, e.g., Kuroda and Yokoyama (1948, 1949), Belin (1959), Sakakura et al. (1959), Stoker and Kruger (1975), Kruger and Warren (1977), Kruger et al. (1977), D'Amore et al. (1978), Warren and Kruger (1979), Warren et al. (1979), and Semprini (1981). Radon has been used for many ground water studies, e.g., Hoogteijling et al. (1948), Miholić (1958); Mazor (1962), Andrews and Wood (1972), Hammond et al. (1977), Martens et al. (1980).

The properties of radon that make it a useful tracer in geothermal reservoirs include a short half-life of 3.82 days, chemical stability as an inert gas, and its continuous production from 1602-year of ^{226}Ra distributed in all geothermal rocks. Parameters providing quantitative data on radon concentration in geothermal fluids include: (1) concentration and distribution of radium in the rock matrix, (2) emanation properties at the rock-fluid interface, and (3) flow conditions of transporting fluids; see, for example, Tanner (1964a,b) and Stoker and Kruger (1975). One of the most uncertain of these parameters is the emanation power, which determines the fraction of radon that escapes from the radium in the host rock and becomes part of the convecting geofluid. The quantitative aspects of radon emanation are especially difficult to determine in the field because measurements are made of wellhead fluids integrating radon emanation over the tansport path through the reservoir. A further complication may be the influence of the fluid transport on the emanation properties of the fractured rock.

In order to obtain a more controlled estimate of the important parameters of radon emanation from fractured rock under geothermal reservoir conditions, several laboratory experiments have been carried out. For example, Macias-Chapa et al. (1980) measured radon emanation under various reservoir conditions of pressure, temperature, and fluid density in a large physical model, using three kinds of pore fluids:

nitrogen, steam, and liquid water. They showed that (1) the rate of radon escape from the rock was greatest with liquid water, (2) for superheated steam, the radon emanation was dependent on the amount of liquid water present within the pore space, and (3) for a single-phase system, radon emanation depended strongly on temperature, but not on pressure. However, Macias-Chapa (1981) also noted that the emanation values decreased under intense heating and cooling cycles of approximately 70 days. This observation was interpreted as a drying effect on the rock combined with an annealing effect caused by curing natural radiation damage through heat treatment. It was not clear which of these two effects, moisture or annealing, is significant in the emanation process.

The process of radon escape from rock is not well understood. The emanation process consists of recoil and diffusion of radon (Flügge and Zimens, 1939). These processes have not been well studied under geothermal conditions of high-temperature and superheated steam. Measurements of the diffusion coefficient of radon in the high temperature range of 150" to 300°C are not available. To examine the recoil and diffusion processes in the emanation of radon, a mathematical model is needed to account for the effects of temperature, pore fluid, and other reservoir parameters. This model will need experimental data on diffusion coefficients determined under various conditions to be compared with values estimated from the model. The development of such a model should prove very useful in the application of radon as an in-situ tracer in geothermal fields.

1.2 OBJECTIVE OF THIS STUDY

The objective of this study is to develop a more quantitative description of the processes responsible for radon emanation from rock in geothermal reservoirs. To achieve this, four major areas of the subject require increased investigation:

1. Rock-size effect: Flügge and Zimens (1939) and Andrews and Wood (1972) showed that the radon emanation power is a function of grain size. Laboratory studies allow the use of measured rock sizes.

2. Annealing effect: Barretto **(1975)** reported a progressive reduction in radon emanation from some minerals by an annealing effect caused by curing of natural radiation damage of the crystalline structure through heat treatment. The importance of the magnitude of the annealing effect on radon emanation needs further clarification.
3. Moisture effect: Tanner **(1978)** reported that water absorbed on interstitial surfaces and condensed by capillary force in pore space can significantly contribute to emanation power, because the range of radon recoil in water is much smaller than that in gas. Compared to gases, water can stop more radon atoms in a given pore space before the atoms penetrate into neighboring grains. The moisture effect on emanation power may be a key one.
4. Recoil and diffusion processes: Both processes are sensitive to pressure, temperature, and fluid properties. In this study, experiments using water-free evacuated and superheated steam conditions provide a relatively simple system to study the contribution of the recoil and diffusion processes to emanation power.

1.3 SCOPE OF THE STUDY

This study evaluates the results of an experimental research program carried out to obtain data on four major areas affecting the magnitude of radon escape from rock particles to pore fluid. These are particle-size effect, annealing effect, moisture effect, and recoil and diffusion processes. The experiments designed for this study examine these areas individually and in combination.

In room-temperature runs, rock size was varied using four graywacke sandstone samples of different particle size. The annealing effect was examined by using one sample of the original sandstone and three samples heat-treated at different temperatures, with dry nitrogen and water *as* pore fluids. From these runs, the influence of annealing and rock size on emanation power was estimated.

In elevated-temperature runs, the Radon Emanation Physical Model developed by Macias-Chapa **(1981)** was used. Smaller high-pressure

vessels were added to the air bath. The large vessels were used for the experiments on buildup of radon under evacuated conditions at several temperatures. The moisture effect was examined in the small vessels. Data from the large vessel experiments were used to test the validity of the emanation model established by Flügge and Zimens (1939). Small amounts of water were added to the small vessels to vary the partial pressure of water vapor under superheated conditions.

Sedimentary rocks, such as graywacke, consist of many types and sizes of mineral grains and cementing materials. These are expected to play a significant role in radon emanation. Microscopic observations of grain size distributions and mineral components in rock particles were obtained to examine the potential for segregation of radium-bearing grains during the rock-crushing step.

Analysis of the experimental data, in conjunction with a theoretical evaluation of the emanation processes, should allow a better estimation of physical characteristics of geothermal reservoirs and assist in the use of radon as an in-situ tracer of reservoir transport and flow processes.

CHAPTER 2

THEORY AND PREVIOUS STUDIES

The process of radon emanation from rock is complex and has been studied by many investigators. Factors involved include the radium source, radon emanation and radon migration. Many studies have been reported on the characteristics of radon and its physical end chemical properties. Theories are available concerning the emanation process due to recoil and diffusion of radon which describe emanation power as a function of time, temperature, pressure, rock size, and pore fluid.

2.1 REVIEW OF PREVIOUS STUDIES

Radon is produced from alpha decay of its parent nuclide. Therefore its source in a rock is determined by the concentration and distribution of radium in the rock. The radon concentration in the rock pore space is determined by the emanating power. Only a small fraction of the radon produced is available as a tracer, because most of the atoms liberated on decay of radium are stopped in the rock. When a radon atom escapes into the pore space through its recoil energy or by diffusion, its migration is controlled by flow properties of the pore fluid. Therefore fluid movement is an important process in determining the radon concentration in produced geofluids.

Migration of radon as a tracer is very sensitive to its surroundings. Many reports of radon in the atmosphere, soil gas, ground waters, petroleum and natural gas have been published (Tanner, 1964a, 1978). In geothermal regions, Kuroda and Yokoyama (1948, 1949) made observations on radon and thoron from hot springs in Japan. Belin (1959) made measurements on these elements associated with gas and condensate samples from fumaroles and pools in New Zealand. Sakakura et al. (1959) and Stoker and Kruger (1975) reported that the concentration of radon in geothermal reservoirs is remarkably influenced by the porosity and fracture conditions in the formation. D'Amore et al. (197'8) conducted a radon survey in wells at Larderello, Italy, and observed considerable variations in concentration. According to their studies, the radon concentration in the fluid is proportional to the radon emanation power

and rock density, but inversely to the rock porosity and fluid density. Kruger et al. (1977) first demonstrated radon concentration dependence on flow rate for a well at the Geysers, in northern California. Radon transient analyses were carried out by Kruger and Warren (1977) and Warren and Kruger (1979). Semprini (1981) performed radon transect analysis to study flow and thermodynamic characteristics of geothermal reservoirs in three reservoirs: the Geysers, California (vapor-dominated), Wairakei, New Zealand (liquid-dominated), and Cerro Prieto, Mexico (liquid-dominated). He found that the average radon concentration in the liquid-dominated reservoirs of Cerro Prieto and Wairakei are 40 times lower than in the vapor-dominated Geysers reservoir. He concluded that the difference between vapor and liquid-dominated systems might be due to the difference in pore fluid density of steam compared to water, which directly affects the rock-fluid ratio for radon emanation. Warren and Kruger (1979) noted that radon emanation power should be a function of rock type, fragment size, pressure, temperature, and pore fluid.

2.2 RADON CHARACTERISTICS

2.2.1 Radioactive Decay of Uranium Series

Three important isotopes of radon exist: ^{219}Rn with a half-life of 3.96 sec, ^{220}Rn with a half-life of 55.6 sec, and ^{222}Rn with a half-life of 3.82 days (Friedlander et al., 1981). These are intermediate daughters of the corresponding ^{235}U, ^{232}Th, and ^{238}U natural radioactive decay series. Since the half-lives of ^{219}Rn and ^{220}Rn are very short compared to the half-life of ^{222}Rn, the use of radon as a tracer in geothermal reservoirs implies the isotope ^{222}Rn.

Uranium has three naturally occurring isotopes: ^{238}U, ^{235}U, and ^{234}U. The abundances of these three isotopes are 99.2739, 0.7204, and 0.0057%, respectively (Faure, 1977). Since ^{222}Rn originates in the most abundant ^{238}U series, it is the most abundant radon isotope in rock. In this decay series, ^{238}U releases eight ^{4}He nuclei, six β^- particles, and 47.4 MeV of energy per atom, ending in stable ^{206}Pb. The overall decay series can be written as

$$^{238}U \rightarrow {}^{206}Pb + 8\ {}^{4}He + 6\ \beta^- + Q \qquad (2\text{-}1)$$

The decay of the uranium series is shown in Fig. 2-1.

^{222}Rn is produced from alpha decay of ^{226}Ra with a half-life of 1602 years in this series.

Radioactive decay

The law of radioactive decay states that the rate of decay of a radionuclide is a first-order process and proportional to the number of atoms (N) present at time (t). It is mathematically expressed as

$$-\frac{dN}{dt} = \lambda N \qquad (2\text{-}2)$$

where λ is the decay constant, characteristic of the particular radionuclide. The half-life of the radionuclide is defined as the time interval for decay of one half of an initial quantity and is expressed by $T_{1/2} = \ln 2/\lambda$.

By integration of Eq. 2-2, the law of radioactive decay is also given as

$$N = N^o\ e^{-\lambda t} \qquad (2\text{-}3)$$

where N^o is the original number of atoms present at time $t = 0$. Equation 2-3 is the basic equation of the radioactive decay process.

Decay series

Let us consider the decay of a parent (N_1) and its radioactive daughter (N_2). The rate of decay of the parent is

$$-\frac{dN_1}{dt} = \lambda_1 N_1 \qquad (2\text{-}4)$$

The rate of decay of the daughter (N_2) is expressed as the difference between the rate at which it is produced by decay of its parent and its own decay rate:

$$\frac{dN_2}{dt} = \lambda_1 N_1 - \lambda_2 N_2 \qquad (2\text{-}5)$$

where

λ_1 = decay constant of the parent nuclide

λ_2 = decay constant of the daughter nuclide

N_1 = number of atoms of the parent remaining at time t

N_2 = number of atoms of the daughter remaining at time t.

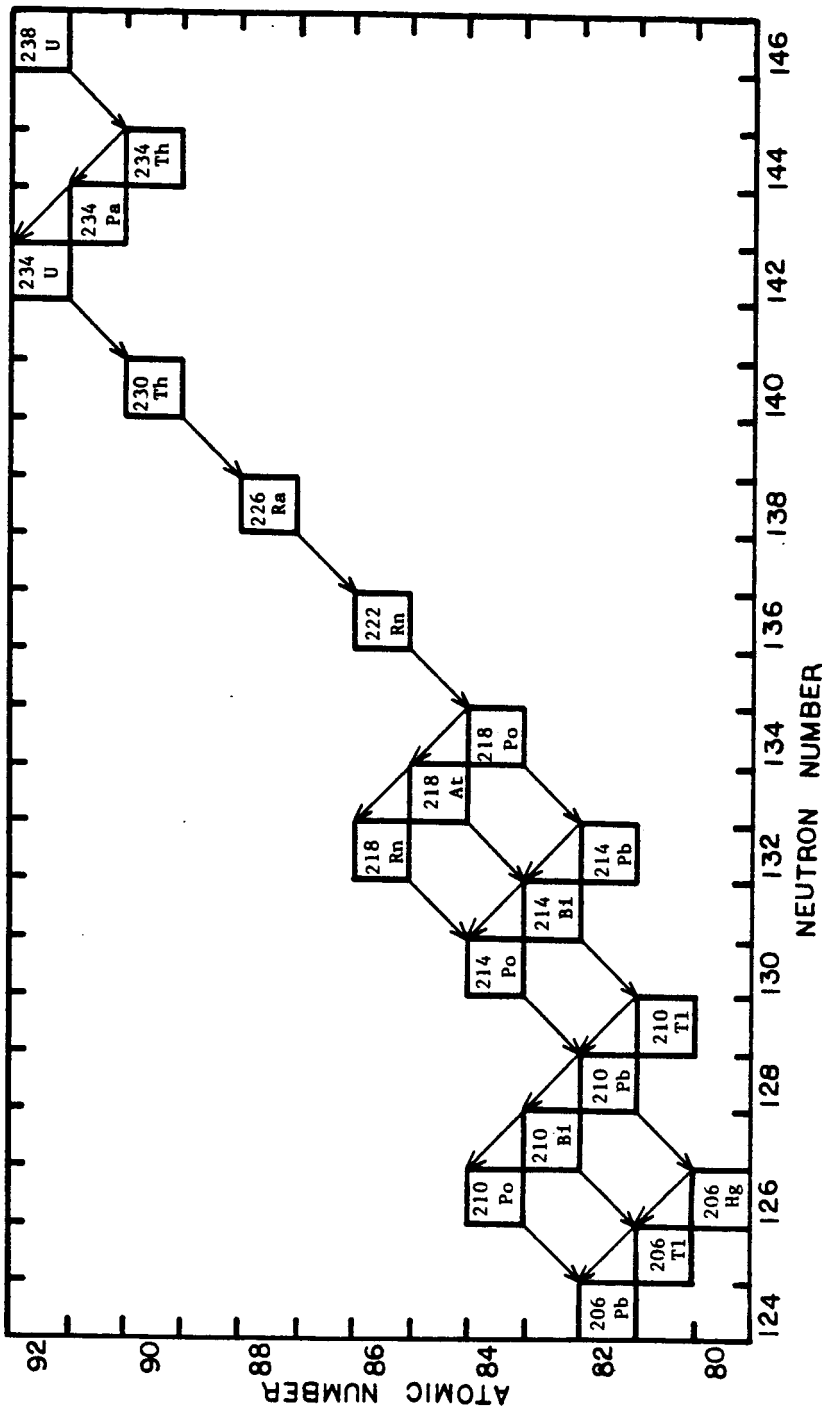

Figure 2-1. The decay of the uranium series.

Substituting Eq. 2-3 into Eq. 2-5 yields a linear first-order differential equation

$$\frac{dN_2}{dt} + \lambda_2 N_2 - \lambda_1 N_1^o e^{-\lambda_1 t} = 0 \qquad (2\text{-}6)$$

The solution to Eq. 2-6 is

$$N_2 = \frac{\lambda_1}{\lambda_2 - \lambda_1} N_1^o (e^{-\lambda_1 t} - e^{-\lambda_2 t}) + N_2^o e^{-\lambda_2 t} \qquad (2\text{-}7)$$

The first term shows the number of daughter atoms which have formed by decay of parent atoms. The second term represents the number of daughter atoms which remain from an initial number N_2^o. Generally N_2^o is zero and Eq. 2-7 reduces to

$$N_2 = \frac{\lambda_1}{\lambda_2 - \lambda_1} N_1^o (e^{-\lambda_1 t} - e^{-\lambda_2 t}) \qquad (2\text{-}8)$$

If $\lambda_1 < X2$, then $e^{-\lambda_2 t}$ will approach zero faster than $e^{-\lambda_1 t}$ as t increases. In such cases, Eq. 2-8 further reduces to

$$N_2 \simeq \frac{\lambda_1}{\lambda_2 - \lambda_1} N_1^o e^{-\lambda_1 t} \qquad (2\text{-}9)$$

From Eq. 2-3,

$$N_1 = N_1^o e^{-\lambda_1 t} \qquad (2\text{-}10)$$

Therefore,

$$N_2 \simeq \frac{\lambda_1}{\lambda_2 - \lambda_1} N_1 \qquad (2\text{-}11)$$

In the naturally occurring uranium, actinium, and thorium series arising from ^{238}U, ^{235}U, and ^{232}Th, respectively, the half-lives of the parent nuclides are very much longer than those of their daughters. Table 2-1 lists the half-lives of the major radioactive Isotopes in the uranium series. Since the decay constant for uranium is much smaller than the decay constant of its daughters, the difference $\lambda_2 - \lambda_1$ in Eq. 2-11 can be replaced by λ_2. Thus the radioactivity of each major daughter product is equal to the uranium radioactivity by

$$\lambda_1 N_1 = \lambda_2 N_2 \qquad (2\text{-}12)$$

Table 2-1

Decay Mode, Half-Life, and Equilibrium Mass of the Uranium Decay Series

Elements in order of decay sequence	Decay mode	Half-life*	Equilibrium mass relative to ^{238}U (grams)
^{238}U	α	4.46×10^{9} y	1
^{234}Th	α	24.10 d	1.20×10^{-11}
^{234}Pa	β^-	6.75 h	1.25×10^{-13}
^{234}U	α	2.45×10^{5} y	5.58×10^{-5}
^{230}Th	α	8.0×10^{4} y	1.85×10^{-5}
^{226}Ra	α	1.60×10^{3} y	3.77×10^{-7}
^{222}Rn	α	3.8235 d	2.51×10^{-12}
^{218}Po	α	3.05 m	1.42×10^{-15}
^{214}Pb	β^-	26.8 m	1.27×10^{-14}
^{214}Bi	β^-	19.7 m	9.33×10^{-15}
^{214}Po	α	1.64×10^{-4} s	1.29×10^{-21}
^{210}Pb	β^-	22.3 y	5.66×10^{-9}
^{210}Bi	β^-	5.01 d	3.48×10^{-12}
^{210}Po	α	138.38 d	9.62×10^{-11}
^{209}Pb	stable	-	-

* From Friedlander et al. (1981).

This relation is known as secular equilibrium. In the naturally occurring radioactive decay series, the condition of secular equilibrium is propagated through the series

$$\lambda_1 N_1 = \lambda_2 N_2 = \lambda_3 N_3 = \ldots \qquad (2\text{-}13)$$

In particular, the pair of most importance is the $^{238}U \rightarrow ^{226}Ra \rightarrow ^{222}Rn$ series. Radium as a homolog of the Ca, Sr, Ba series can thermochemically separate from uranium. However, because of its relatively long half-life of 1600 years, the production rate of radon will be in secular equilibrium with radium and its occurrence will be determined by the concentration and distribution of its parent radium.

2.2.2 Physical and Chemical Properties

Radon was discovered in 1900 by Dorn, who called it radium emanation (Weast and Astle, 1981). It is the heaviest known gaseous element with a density of 9.73 g/ℓ at 273K, 1 atm. In addition to the three natural isotopes, 22 isotopes of radon have been synthesized by nuclear reactions in cyclotrons and linear accelerators, but none of these is as long-lived as ^{222}Rn (Parker, 1982). Radon possesses a particularly stable electronic configuration and has the chemical properties characteristics of noble-gas elements: helium, neon, argon,, krypton, and xenon. Radon can, however, react with fluorine to form radon fluoride (Weast and Astle, 1981).

Table 2-2 lists some of the physical properties of radon (from Cook, 1961). Radon is readily adsorbed on charcoal, silica gel, and other adsorbents, and this property can be used to separate it from other gases. Radon is appreciably soluble in water and many organic solvents, such as toluene. The solubility of radon gas in water is shown in Fig. 2-2 (Clever, 1979). According to Rogers (1958), radon solubility is remarkably reduced when electrolytes are in solution.

Table 2-2
Properties of Radon*

Atomic weight		ca. 220
Atomic number		86
Melting point		-71°C
Boiling point		-61.8°C
Density of gas		9.73 g/ℓ
Specific gravity:	liquid	4.4 at -62°C
	solid	4
Valence		± 0

* From Cook (1961).

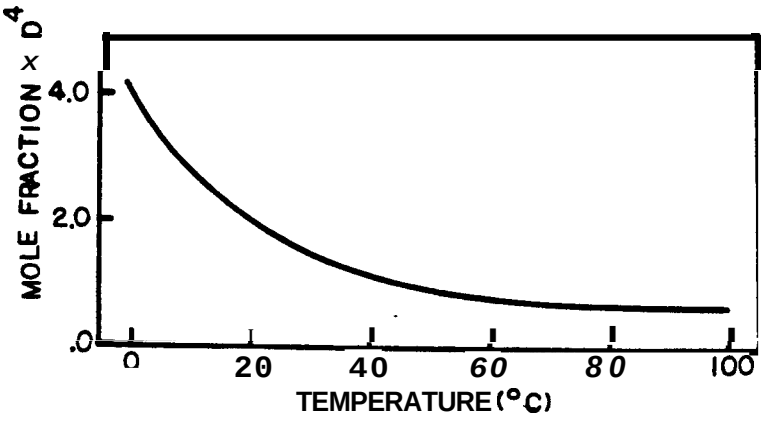

Figure 2-2. The solubility of radon in water as a mole fraction at a partial pressure of 1 atm (from Clever, 1979).

2.3 THEORY OF THE EMANATION PROCESS

Hahn and Müller (1923) defined emanation power as the fraction of radioactive inert-gas atoms formed in a sclid that escapes from the solid. When a large fraction of such gas escapes, the substance is called a highly emanating material.

On the other hand, Kapustin and Zaborenko (1974) determined the emanating capacity of solids as the emanation coefficient E, which consists of the sum of the probabilities of the escape of inert gas atoms from the solid as a result of radioactive recoil process, E_R, and diffusion process, E_D. In either case, the emanation power EP, used in this report, depends on the mineral composition, crystal structure, specific surface area, temperature, moisture and water content, and homogeneity of the substance. It depends also on the diffusion coefficient, the recoil energy, and the half-life of the radioactive inert gas.

2.3.1 Emanation Power Due to Recoil

The emanation process due to recoil results when a parent radium atom decays by alpha-particle emission; the resulting radon atom must recoil in the opposite direction to conserve momentum. The recoil energy may be sufficient to carry it from the solid to the surroundings. Flügge and Zimens (1939) established a theory of emanation power, assuming that a single grain containing the parent radionuclide is

homogeneous and isotropic. Their theory is also based on a grain of sufficient age, that the rate of the inert-gas formation is equal to the sum of its decay rate within the grain and its escape rate from the grain. Under these assumptions, steady-state conditions are established in the formation. A summary of this theory is given by Wahl (1951) for a spherical grain of radius r_o, large compared to the recoil range R of a ^{222}Rn atom. According to Quet et al. (1975), the recoil atoms of radon have a range from 20 to 70 nm in homogeneous minerals. The above assumption may be valid since grain sizes are typically of the order of 1 μm or larger.

Figure 2-3 shows a schematic diagram of direct recoil from a solid sphere (Flügge and Ziemens, 1939). The geometric loss P(x) for the recoil atom is defined as the ratio of the surface area of the spherical plane ABC to the surface area of the sphere of radius R and is given by

$$P(x) = \frac{2\pi R(R - X)}{4\pi R^2} = \frac{R - x}{2R} \qquad (2\text{-}14)$$

where x is expressed as $x = (r_o^2 - R^2 - r2)/2r$. When the parent atom is located on the surface of a grain (x = 0), P(x) is equal to 0.5. On the

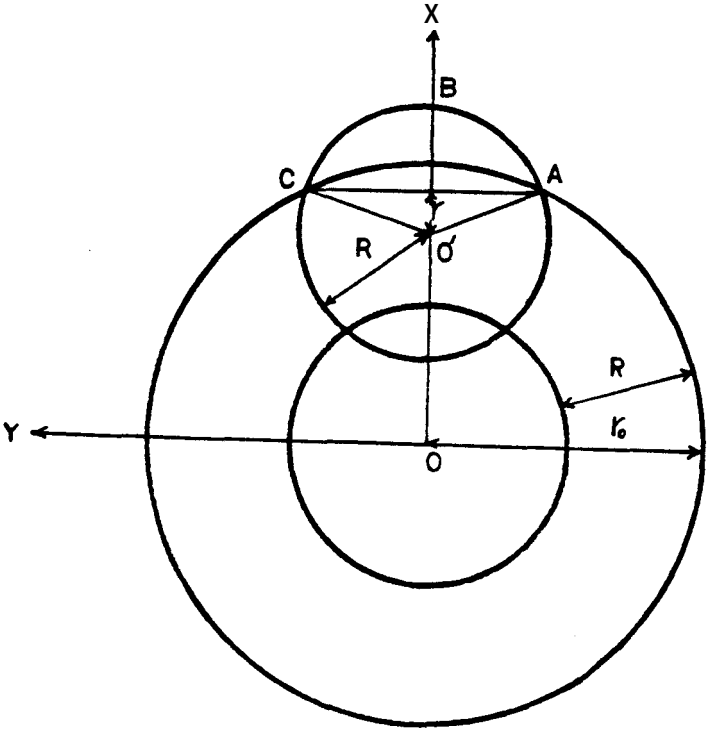

Figure 2-3. Schematic diagram of direct recoil from a spherical grain.

other hand, when $x \geq R$, the radium atoms located in that region cannot contribute to emanation power of the grain.

Substitution of the expression for x into Eq. 2-14 reduces to

$$q(r) = \frac{2Rr - (r_o^2 - R^2) + r^2}{4Rr} \tag{2-15}$$

The production rate of escaped recoil atoms N_R is

$$N_R = c_1 \lambda_1 \, 4\pi \int_{r_o - R}^{r_o} q(r) r^2 \, dr \tag{2-16}$$

where

c_1 = concentration of radon

λ_1 = decay constant of radium

$c_1 \lambda_1$ = production rate of daughter atoms per unit volume.

The solution of Eq. 2-16 is

$$N_R = c_1 \lambda_1 \pi (R r_o^2 - \tfrac{1}{12} R^3) \tag{2-17}$$

The total production rate of recoil atoms N is

$$N = \frac{4}{3} \pi r_o^3 c_1 \lambda_1 \tag{2-18}$$

The emanation power due to recoil E_R is

$$E_R = \frac{c_1 \lambda_1 \pi (R r_o^2 - \frac{1}{12} R^3)}{\frac{4}{3} \pi r_o^3 c_1 \lambda_1}$$

$$= \frac{3}{4} \frac{R}{r_o} - \frac{1}{16} \left(\frac{R}{r_o}\right)^3 , \quad 2r_o \geq R \tag{2-19}$$

Since the second term in Eq. 2-19 can be negligible for large grains, ($r_o >> R$), Eq. 2-19 may be reduced to

$$E_R = \frac{3}{4} \frac{R}{r_o} \tag{2-20}$$

Equation 2-20 shows that the emanation power due to recoil is given by

$$E_R = \frac{R}{4} \times \left(\frac{\text{grain surface area}}{\text{grain volume}}\right) \tag{2-21}$$

For example, in grains of 1 μm radius containing ^{226}Ra with a radon recoil range of 36 nm, E_R will be 2.7%, as reported by Heckter (1934).

2.3.2 Emanation Power Due to Diffusion

The second major process for emanation of radon from single grains is diffusion. The effects of diffusion can be evaluated from Fick's law' and a mass balance equation.

Fick's first law

According to Fick's first law, the rate of transfer of diffusing molecules through a unit area is proportional to the concentration gradient measured normal to the area (e.g., Shewman, 1963). Fick's law is given by

$$J = - D \frac{\partial C}{\partial x} \qquad (2\text{-}22)$$

where

J = flux of diffusing molecules (g/cm^2-sec)
C = concentration of diffusing molecules (g/cm3)
x = space coordinate measured normal to the area (cm)
D = diffusion coefficient (cm2/sec).

The emanation power due to diffusion E_D is defined in a manner analogous to Eq. 2-21 as

$$E_D = - \frac{D \times (\text{particle surface area})}{C_1 \lambda_1 \times (\text{particle volume})} \left(\frac{\partial c}{\partial r}\right)_{r=r_o} \qquad (2\text{-}23)$$

where $\left(\frac{\partial c}{\partial r}\right)_{r=r_o}$ is the concentration gradient of radon at the particle, surface.

Mass balance equation

To calculate the concentration of radon, C_2, as a function of particle radius, r, and time, t, we can establish the following differential equation based on Fick's second law and a mass balance:

$$\frac{\partial C_2}{\partial t} = D\nabla^2 C_2 + C_1 \lambda_1 - C_2 \lambda_2 - C_1 \lambda_1 q(r) \qquad (2\text{-}24)$$

where

DV^2C_2 = diffusion rate of radon
$C_1 \lambda_1$ = production rate of radon

$C_2\lambda_2$ = decay rate of radon

$q(r)$ = geometric loss due to the particle size r.

We can redefine the geometric loss $q(r)$ in Eq. 2-24 more precisely as

$$q(r) = \begin{cases} 0 & , \ 0 < r \leq r_o - R \\ \dfrac{Rr + r^2 - r_o^2 + R^2}{4Rr} & , \ r_o - R \leq r < r_o \end{cases} \qquad (2\text{-}25)$$

In Eq. 2-25 the rate of change of radon with time, $\partial C_2/\partial t$, is expressed solely as a function of particle radius r.

Steady-state condition

If the radon concentration is constant with time under steady-state conditions, Eq. 2-24 can be changed to an ordinary differential equation:

$$D\nabla^2 C_2 - C_2\lambda_2 + C_1\lambda_1(1 - q(r)) = 0 \qquad (2\text{-}26)$$

For a spherical rock, Eq. 2-26 can be reduced according to Crank (1975) to

$$\frac{d^2 C_2}{dr^2} + \frac{2}{r}\frac{dC_2}{dr} - \frac{\lambda}{D} C_2 = g(r) \qquad (2\text{-}27)$$

where

$$g(r) = \begin{cases} -\dfrac{C_1\lambda_1}{D} & , \ 0 < r \leq r_o - R \\ -\dfrac{C_1\lambda_1}{D}\left(q(r) - 1\right) & , \ r_o - R \leq r < r_o \end{cases} \qquad (2\text{-}28)$$

Equation 2-27 can be solved for the boundary conditions $C_2(0) < \infty$ and $C_2(r_o) = C_s$, where C_s = concentration of radon at the surface. Kapustin and Zaborenko (1974) give as the solution:

$$C_2(r) = \frac{C_1\lambda_1}{\lambda_2} + \frac{C_1\lambda_1}{2R\lambda_2}\left\{\frac{\cosh\theta}{\sinh\theta}\left[\frac{1}{\omega^2}\cosh\theta - \frac{r_o}{\omega}\sinh\theta\right]\right.$$

$$- \frac{1}{\omega^2}\frac{1}{\sinh 8} + \frac{1}{\sinh \omega r_o}\left[\frac{1}{\omega^2} + Rr_o a - \frac{R(2r - R)}{2}\right.$$

$$\left.\left. - \left(\frac{\cosh\theta}{\omega^2} - \frac{r_o}{\omega}\sinh w(r_o - R)\right)\cosh \omega r_o\right]\right\}\frac{\sinh \omega r}{r},$$

$$0 < r \leq r_o - R \qquad (2\text{-}29)$$

$$C_2(r) = \frac{C_1\lambda_1}{4R\lambda_2}\left(2R - r - \frac{2}{\omega^2 r} + \frac{r_o^2 - R^2}{r}\right) + \frac{C_1\lambda_1}{2R\lambda_2}\frac{1}{\sinh \omega r_o}\left[\frac{1}{\omega^2}\right.$$

$$\left. + Rr_o a - \frac{R(2r_o - R)}{2} - \left(\frac{1}{\omega^2}\cosh 8 - \frac{r_o}{\omega}\sinh\theta\right)\cosh \omega r_o\right]$$

$$\frac{\sinh \omega r}{r} + \frac{C_1\lambda_1}{2R\lambda_2}\left[\frac{\cosh\theta}{\omega^2} - \frac{r_o \sinh\theta}{w}\right]\frac{\cosh \omega r}{r},$$

$$r_o - R \leq r < r_o \qquad (2\text{-}30)$$

where

$$\omega^2 = X/D$$

$$a = 2C_s\lambda_2/(C_1\lambda_1)$$

$$8 = \omega(r_o - R).$$

By introducing $a = R/r_o$ and $\beta = \omega r_o$, the emanation power due to diffusion E_D is

$$E_D = \frac{3}{2\beta^2}\left\{\frac{1}{a} - 1 + a + \coth\beta\left[\beta(1 - a) - \frac{1}{\alpha\beta} - \frac{\alpha\beta}{2}\right.\right.$$

$$\left.\left. - \frac{\sinh B(1 - a)}{a\sinh\beta} + \frac{\cosh(1 - \alpha)}{\alpha\beta\sinh\beta}\right]\right\} \qquad (2\text{-}31)$$

For large particles, α is usually less than one and Eq. 2-31 may be simplified for the case of $\beta \gg 1$ to

$$E_D = \frac{3(2 - a)}{2\beta} \qquad (2\text{-}32)$$

and for $a \ll 1$ to

$$E_D = \frac{3}{\beta} \tag{2-33}$$

2.3.3 Overall Emanation Power

Since the overall emanation power, E, consists of the sum of the recoil and diffusion processes, E has the form of

$$E = E_R + E_D = \frac{3a}{4} + \frac{3(2 - a)}{26} \tag{2-34}$$

On the assumption that the surface concentration of radon, C_s, is small, for example in the case of systems in which radon atoms are continually swept from the rock surface, $a = 0$ and Eq. 2-34 can be simplified further to

$$E = \frac{3\alpha}{4} + \frac{3}{\beta} \tag{2-35}$$

This expression is the equation derived by Flügge and Zimens (1939) for the emanation power due to diffusion through a large particle ($E_R < 0.5\%$),

$$E_D = \sqrt{\frac{D}{\lambda_2}} \left(\frac{\text{particle surface area}}{\text{particle volume}}\right)$$

$$= \sqrt{\frac{D}{\lambda_2}} \rho \left(\frac{\text{particle surface area}}{\text{particle mass}}\right) \tag{2-36}$$

where ρ is the density of the particle.

2.3.4 Buildup of Emanation Power

When the half-life of the parent nuclide is much longer than that of its daughter ($\lambda_1 \ll \lambda_2$), Eq. 2-8 can be given as

$$N_2 = \frac{\lambda_1 N_1^o}{\lambda_2} \left(1 - e^{-\lambda_2 t}\right) \tag{2-37}$$

For ^{226}Ra and ^{222}Rn in solution, the radioactivity of radon $[A_{Rn}]$ is given by

$$[A_{Rn}] = [A_{Ra}] \left(1 - e^{-\lambda_2 t}\right) \tag{2-38}$$

where

$[A_{Ra}]$ = radioactivity of radium

λ_2 = decay constant of radon

t = time.

Equation **2-38** shows an exponential buildup of radon with time and secular equilibrium is established after a period of approximately **30** days. For radium atoms in a crystalline material, $[A_{Rn}]$ is also dependent on the emanation power E from the crystals. Thus,

$$[A_{Rn}] = E[A_{Ra}] \left(1 - e^{-\lambda_2 t}\right) \qquad \textbf{(2-39)}$$

When the radioactivity of radon and radium in a system is known, the emanating power can be estimated by Eq. **2-39.** Repeated measurements can determine if steady-state conditions exist **so** that emanation power is independent of time.

2.3.5 Temperature Dependence of Emanation Power

Temperature is an important parameter in radon emanation with respect to the two release processes of recoil and diffusion. Since radioactive decay is essentially independent of temperature, the recoil process should not be affected by temperature changes. On the other hand, as the diffusion coefficient is a function of temperature, the diffusion process should be affected by temperature fluctuation.

Glasstone et al. **(1941)** and Shewman **(1963)** noted that the diffusion coefficient can be described empirically by an equation similar to the Arrhenius equation:

$$D = A \exp\left(-\frac{Q_D}{RT}\right) \qquad \textbf{(2-40)}$$

where

A = empirical constant (cm^2/sec)

Q_D = activation energy of diffusion (J/mol)

R = gas constant (J/mol-K)

T = Kelvin temperature (K).

In this equation, both A and Q_D are independent of temperature.

It was noted in Eq. 2-36 that the emanation power due to diffusion, E_D, is proportional to $\sqrt{D}$. Thus the temperature dependence of the emanation power due to diffusion can be expressed as

$$E_D = k\sqrt{D} \tag{2-41}$$

where $k = 3\sqrt{1/(\lambda_2 r_o^2)}$.

From Eqs. 2-40 and 2-41,

$$E_D = k\sqrt{A \exp\left(-\frac{E}{RT}\right)}$$

$$= k A' \exp\left(-\frac{E}{RT}\right) \tag{2-42}$$

where

$A' = \sqrt{A}$;

$Q_E = Q_D/2$ or the experimental activation energy.

Experimentally Q_E and A' may be obtained from a plot of $\ln E_D$ vs $1/T$. The linear curve is expressed as

$$\ln E_D = \ln k A' - \frac{Q_E}{R}\frac{1}{T} \tag{2-43}$$

The slope is given by

$$\frac{d \ln E_D}{d \frac{1}{T}} = -\frac{QE}{R} \tag{2-44}$$

while Rn k A' is given by the intercept at $1/T = 0$. A and Q_D can be determined from A' and Q_E calculated from the intercept and slope of the curve, and the diffusion coefficient D can be estimated as a function of temperature.

2.3.6 Pressure Effect of Emanation Power

Although temperature is a primary parameter for diffusion rates, pressure may also cause a variety of effects on radon emanation. Yund and Anderson (1978) pointed out that oxygen diffusivity in a deep formation increased by a factor of 10 as water pressure increased from 125 to 4000 bar. These data were explained in terms of an increased activity of the water in the feldspar and by the operation of an intra-crystalline hydrolysis reaction mechanism.

Giletti and Tullis (1977) could not detect any change in Ar diffusion coefficients in phylogopite under hydraulic pressures between 2 and 15 kbar. Newton and Round (1961) discussed the effect of diffusion on the migration of helium in sediments. In their mathematical model, they

assumed the effect of pressure on diffusion was very small since water filling the major part of the pore space is very incompressible.

Pressure change in a two-phase geothermal system may affect the water saturation and fluid density in the rock pore space. Kruger et al. (1978) noted an increase in radon concentration with temperature decline under pressurized production in the LASL Hot Dry Rock Project, Phase 1 test. They suggested that the induced pressure may have been one of the controlling factors on radon emanation history observed during the test.

Macias-Chapa (1981) found that for a single-phase pore-fluid, e.g., water or nitrogen, radon emanation depended strongly on temperature, but not very strongly on pressure in the pressure range studied, 1 to 21 atm.

The pressure effect on radon emanation is as yet uncertain. For a single-phase pore fluid, it seems to be less significant, but more complicated for two-phase fluids.

2.3.7 Rock Size Effect on Emanation Power

Since the two main processes of recoil and diffusion are functions of particle size, radon emanation power is expected to be dependent on particle size over some range. Andrews and Wood (1972) investigated the dependence of total radon released into the water phase on rock particle! size in water-rock systems by using rocks of varied particle size. Their results showed that radon release is proportional to $1/\sqrt{d}$, although the surface area per unit volume is inversely proportional to the mean diameter of particles, d. They explained that the integrated grain boundary length intersecting the surface is proportional to the square root of the surface area for rock particles in which grains are uniformly distributed, and therefore radon emanation power should be proportional to $1/\sqrt{d}$.

They also estimated that the emanation power reached 100% for particles less than 1 μm in diameter from extrapolation of the relation between emanation power and particle size. However, according to Eq. 2–24, particles of 1 μm in diameter should result in emanation power due to recoil of only 2.7%. This significant difference in estimated emanation power cannot be explained by the difference between the $1/d$ and $1/\sqrt{d}$ relationships alone. Thus mineralogical and petrographic

explanations are needed to investigate the grain size distribution and to examine the radium-bearing minerals and cementing materials.

2.3.8 Annealing Effect of Emanation Power

Annealing is defined as a process in which residual sttresses and accumulated strains are reduced or eliminated under appropriate conditions (Stanton, 1972).

When a rock is heated to the temperature threshold above atomic mobility, crystal lattices may be rearranged to be strain-free. On the other hand, radioactive decay may cause damage to the crystal. structure.' Tanner (1978) pointed out that the effect of radiation damage is to form a mosaic of channels in which water may be introduced. One result may be an increase in the direct recoil fraction of emanating power. Another may be an increase in indirect recoil and diffusion. When optimum conditions prevail for the diffusion and recoil processes of radon through damaged zones, the emanation power of radon may increase to some extent. From high-temperature experiments (up to 1200°C) on minerals, Barretto (1975) reported a progressive decrease in radon emanation as temperature increased. He explained the observation as the result of annealing of natural radiation damage. Tanner (1978) also cited the work of Lambert et al. (1972) and Lambert and Bristeau (1943) in which radiation damage alone did not significantly increase radon escape by diffusion.

Since the annealing process would accompany some crystal rearrangements, microscopic observation of rocks may be needed in addition to measurements of radon emanation. However, it is more important to determine whether the annealing effect on radon emanation from a given rock is significant.

2.3.9 Pore-Fluid Dependence on Emanation Power

Radon emanation power may be affected by the kind of fluid occupying the pore spaces. A condensable gas, such as water vapor, is expected to affect emanation power because its phase condition is quite dependent on temperature and pressure. In a two-phase system of water and steam, the radon emanation behavior will be more complfcated, because capillary force and water adsorption affect each phase differently

in a porous medium, and the radon emanation mechanism may be quite different.

When diffusion is the major process for radon emanation in a one-phase system, temperature changes may cause significant changes in emanation, independent of pressure, because water is much more incompressible than gases. Macias-Chapa (1981) reported that for single-phase pore fluids, radon emanation depended strongly on temperature but not very much on pressure. However, he noted a large experimental error in the pressure measurements.

CHAPTER 3

EXPERIMENTAL METHODS

The graywacke sandstone used in these studies was the same graywacke used in previous studies by Macias-Chapa **(1981).** Some of the original sandstone were used directly after they were crushed and sieved, into several size ranges. Other aliquots were first annealed by heating at temperatures ranging from 120" to 500°C and slowly cooled to room temperature. Room-temperature runs were carried out in 2-liter flasks in which the rock samples were sealed with dry nitrogen or water as the pore fluid. After buildup, radon was swept from the flask to the analytical system through glass tubing. A schematic view of this system is shown in Fig. **3-1.**

The elevated-temperature runs were carried out in the three **13.5-R** reservoirs in the Radon Emanation Physical Model constructed by Macias-Chapa **(1981).** Radon was swept after buildup to the analytical system using the built-in sweep piping. In this study three additional smaller, high-pressure vessels were added to the model. Two were 500 mℓ and one was **1000** mℓ in capacity. Radon emanation was measured under controlled conditions of temperature and steam pressure in these reservoirs.

Radon measurements were made using the very efficient and reliable ZnS alpha-scintillation flasks described by Lucas **(1964).** The analytical system for purification of radon by adsorption on activated charcoal and transfer to the scintillation flasks was described by Stoker **(1974).** Details of the experimental methods and data statistics for the series of runs are given in the following sections.

3.1 PREPARATION OF ROCKS

3.1.1 Crushing and Sieving

The dimensions of the graywacke sandstone measured by Macias-Chapa **(1981)** are shown in Table **3-1.**

The original rocks were dried and crushed in a ball mill. The output was separated into mesh size ranges through Taylor sieves. The resulting range of particle sizes of the ground rocks is shown in Table 3-2.

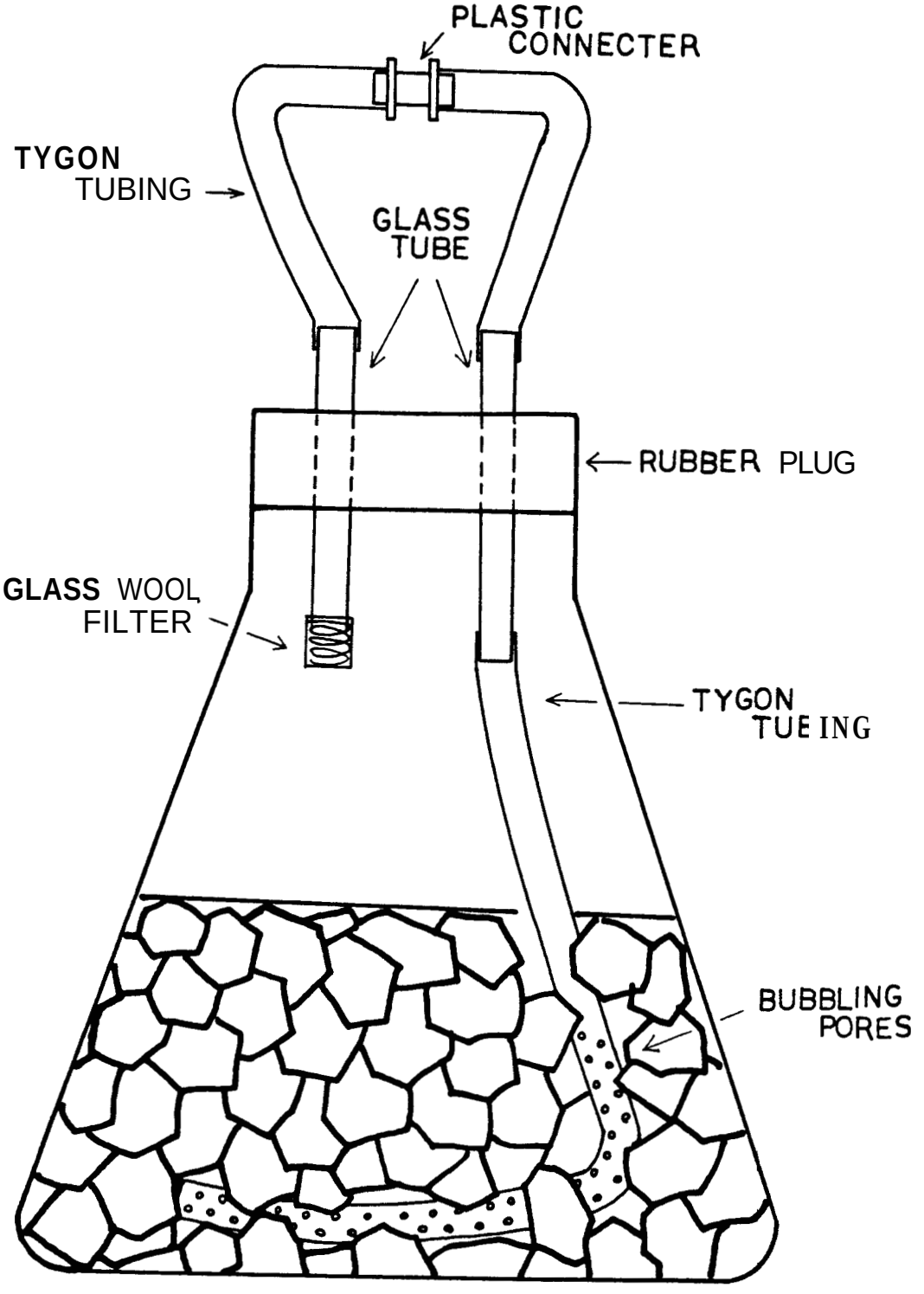

Figure 3-1. Schematic view of a flask loaded with rock.

Table 3-1

Dimensions of the Graywacke Sandstone*

Length (cm)	1.85 ± 0.40
Width (cm)	1.20 ± 0.25
Thickness (cm)	0.67 ± 0.22
Surface area/rock (cm^2)	4.85 ± 0.90
Surface area (cm^2/g)	2.65 ± 2.03

*From Macias-Chapa (1981).

Table 3-2

Size Ranges of Crushed Rocks

Taylor Sieve	Size (mm)
3/8"-5/16"	9.50-8.00
No. 5-No. 14	4.00-1.40
No. 40-No. 120	0.425-0.125
No. 120	< 0.125

Particles finer than 420 μm were separated by wet-sieving to prevent coaggregation in the Taylor sieves. Since the size distribution of each size range except the finest was not determined quantitatively, the median of the upper and lower mesh sizes was adopted as the average rock size of each range. The average size of the original rocks was calculated by the method of Hunsbedt et al. (1975) for spherical particles, in which

$$A = \left(\frac{b + c}{4b}\right)\left[b^2 + \frac{a \cdot b}{1 - \left(\frac{b}{a}\right)^2} \sin^{-1}\left(1 - \left(\frac{b}{a}\right)^2\right)\right] \qquad (3\text{-}1)$$

where

A = surface area (cm^2);

a = length (cm);

b = width (cm;

c = thickness (cm).

3.1.2 Baking and Annealing

A loading of the original rock was annealed by baking for two days at 120°, 300°, and 500°C and then slowly cooling to room temperature. The change in weight due to water loss was measured as a function of temperature. The data are given in Table 3-3.

Table 3-3

Annealing Temperatures and Weight Loss of Rocks

Temperature (°C)	Weight Loss (%)
120	0.79
300	0.82
500	0.83

3.2 ROCK PROPERTIES

According to Gary et al. (1972), graywacke has several definitions, but is now generally described as a dark and very hard, tough, and firmly indurated, coarse-grained sandstone which has subconchoidal fractures and consists of poorly sorted and extremely angular to subangular grains of quartz and feldspar with an abundant variety of small, dark rock and mineral fragments.

The rock used in this study is an igneous metamorphic rock of Western California noted to be from somewhere in the Franciscan formation north of San Francisco, California, but the exact source of the particular rock is not known.

The characteristics of this graywacke sandstone, except for its porosity, were given by Macias-Chapa (1981). The porosity was determined for this study by measuring the weight difference between completely dried and fully wetted rocks. Table 3-4 shows a summary of the graywacke sandstone characteristics. Microscopic observations of this rock are given in Chapter 4.

Table 3-4

Average Rock Characteristics of the Original Graywacke Sandstone

Radium content (1)*	0.61 ± 0.08 pCi/g rock
Density (2)*	2.78 ± 0.73 g/cm3
Weight*	1.83 ± 0.8 g/rock
Surface area (3)*	2.65 ± 1.03 cm^2/g
Specific surface area (4)*	2.8 m^2/g
Water content (up to 500°C)	0.83%
Porosity (2)	4.9 ± 1.3%

*From Macias-Chapa (1981).

(1): measured by the LFE, Environmental Analysis Laboratories, Richmond, CA, and the Los Alamos Scientific Laboratories, Los Alamos, NM.
(2): by a fluid displacement method.
(3): by the method of Hunsbedt et al. (1975).
(4): by the BET method using nitrogen.

3.3 MICROSCOPIC OBSERVATION

To understand the granular characteristics affecting the observed changes in emanation power with heat treatment, microscopic examination of thin sections was obtained.

Ten thin sections of representative samples of the pre-annealed and annealed rocks were made for petrographic observations. The samples were prepared by Mr. Ruperto Laniz, School of Earth Sciences, Stanford University. Microscopic observations were done through a polarized microscope by Dr. Shigenori Maruyama, Geology Department, Stanford University.

3.4 EXPERIMENTAL PROCEDURES

Radon emanation measurements consisted of cold and hot runs. The cold runs were carried out at room temperature using tightly sealed glass flasks. The hot runs were made in high-pressure steel vessels.

3.4.1 Cold Runs

Annealing tests

Three charges of 2 kg of the original graywacke sandstone were annealed by baking and cooling, as described above. Three of the

annealed rock samples and a similar amount of the original rock were placed in 3-liter flasks which have a rubber stopper equipped with inlet and outlet tubes (see Fig. **3-1).**

Each flask was evacuated and dry nitrogen was introduced at atmospheric pressure. The flasks were tightly sealed for 30 days to establish secular equilibrium between ^{226}Ra and ^{222}Rn. The radon gas was flushed from the flask by helium as a carrier gas and adsorbed on an activated-charcoal trap at dry-ice temperature. Each of these experiments was done in triplicate to improve the statistical reproducibility of the data.

On completion of the dry-nitrogen runs, the flasks were filled with water to the top of the rock loading and the test was repeated, again in triplicate.

Rock size test

Four charges of 1.0 kg of the **9.5-8.0** mm rock, **0.5** kg of the 4.0-1.4 mm rock, 0.5 kg of the 0.425-0.125 mm rock and 0.5 kg of the < 0.125 mm rock were placed in glass flasks. To eliminate adsorbed moisture, the rock was baked to constant weight at 120°C for two days. Triplicate experiments were carried out with the same procedure as with the annealing tests with both dry nitrogen and water.

3.4.2 Elevated-Temperature Runs

Buildup tests

Buildup tests were run to investigate the importance of radon diffusion processes under dry and evacuated conditions in the three large vessels. The original rock loading in place for four years fori the experiments by Macias-Chapa **(1981)** were used in the first experiment. Since these rocks had been used with water and steam as pore-fluids, they were dried for several months at 300°C prior to the current experiments.

The set of hot runs was carried out in a manner similar to that reported by Macias-Chapa **(1981),** but modified to yield additional data. A schematic drawing of the revised system is shown in Fig. 3-2. The three large vessels are constructed of 60 kg of 2.5-cm thick carbon steel with flanges, two high-temperature bellow valves, and three internal-flow distribution aluminum baffles. The details of the vessels

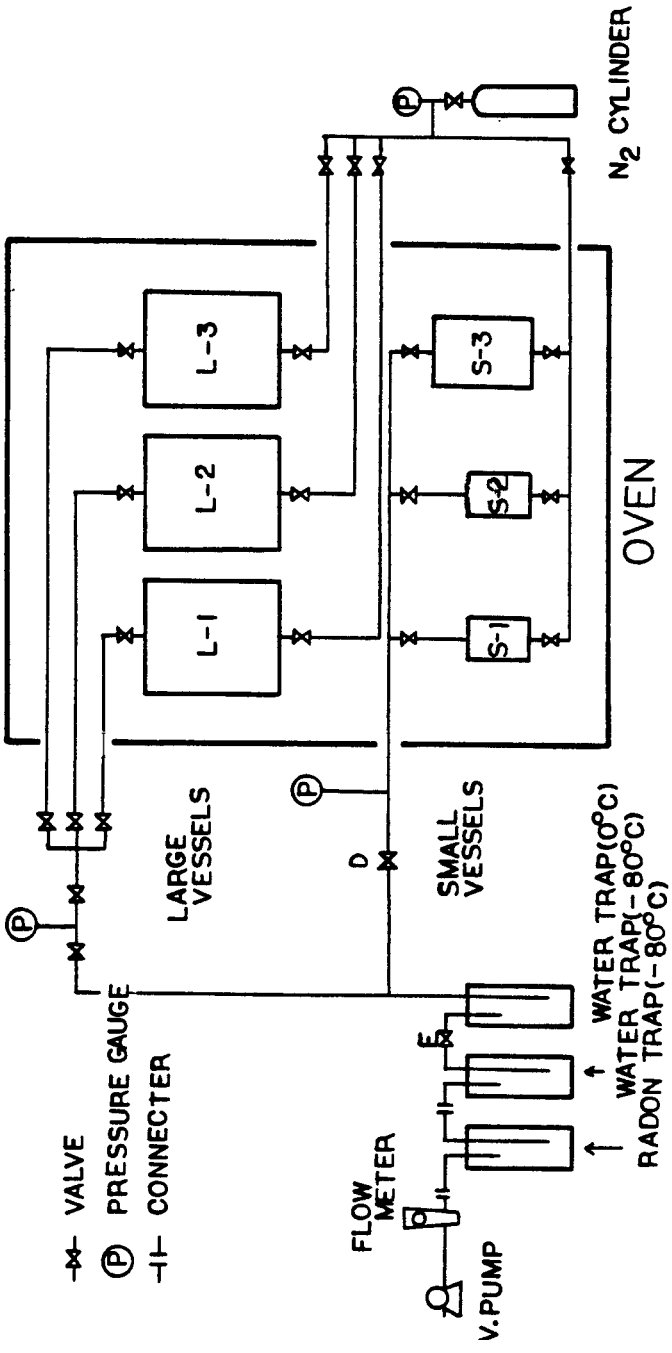

Figure 3-2. Schematic drawing of the physical model.

were reported by Macias-Chapa (1981). Table 3–5 shows the rock loading data. The packed porosity was determined by volume displacement for each vessel.

Table 3–5

Rock-Loading Conditions of Large Vessels*

Vessel No.	Rock Loading (kg)	Packing Porosity (%)
L-I	17.0	54.0
L-II	16.5	56.0
L-III	17.0	54.0

* From Macias-Chapa (1981).

Moisture tests

The moisture tests were carried out to investigate the effect of moisture on radon emanation from rock. For these tests, three smaller vessels were added to the air bath. They consisted of commercially available sampling cylinders fabricated from stainless steel. Two of them have a capacity of 500 mℓ (Matheson Model 4HD500) and one has a capacity of 1000 mℓ (Matheson Model 8HD1000). A bellows valve (Nupro Model SS-4HS) was attached on each end and glass wool was packed between the valve and the vessel to prevent powder contamination.

A schematic drawing of the system is shown in Fig. 3–2 and the rock-loading data are given in Table 3–6.

Table 3–6

Rock Loading Conditions of Small Vessels

Vessel No.	Vessel Capacity (mℓ)	Rock Loading (kg)	Packing Porosity (%)
S-I	500	0.5	64.0
S-II	500	0.5	64.0
S-III	1000	1.0	64.0

The particle size of the small-vessel loading was between 9.5 and 8.0 mm. An amount of water calculated from steam tables by Reynolds (1979) was added to each vessel to maintain a saturated humidity for each temperature.

3.5 RADON EXTRACTION

3.5.1 Cold Runs

The radon extraction system, shown in Fig. 3-3, is basically as described in previous studies (Stoker, *1974;* Macias-Chapa, 1981). The first cold trap was filled with copper ribbon to remove water. The second cold trap was filled with 20 g of activated charcoal, 7-14 mesh in size, to adsorb the radon. In the cold runs, helium was used as the carrier gas. The cold traps were degassed, evacuated and cooled to -80°C in the Freon-dry ice Dewar flasks.

The system was swept by slowly opening the 3-way stopcock (A, B, and C in Fig. 3-3) and adjusting the flow with the flow meter and pinch cocks. The system was swept for 20 min at a helium flow rate of 1-1.5 ℓ/min under suction using the vacuum pump. At the end of the sweep process, the flask was re-evacuated to vacuum. In this sweeping process, the radon gas is selectively adsorbed in the charcoal trap.

3.5.2 Elevated-Temperature Runs

Nitrogen was used as a carrier gas in the elevated-temperature runs. The piping and fittings are made of stainless steel, except the -80°C cold traps, of which one was fitted with copper turnings and one with charcoal. The procedure for the small-vessel runs started by evacuating the system with valves E and D closed before sweeping (Fig. 3-2). The valves of the vessels and the nitrogen cylinder were opened, and nitrogen gas was introduced at a pressure of 20 psig. The nitrogen-cylinder valve was closed and valve D was opened. Valve E was opened gradually to keep the flow rate at about 0.5 ℓ/min. Finally, valve E was fully opened and the sweep was stopped when the flow meter showed no flow. This procedure, repeated twice for each vessel, took about 6 to 8 min for complete evacuation. After sweeping, all valves were closed, and the charcoal trap was sealed off by clamps and detached from the system for radon analysis. The same procedure was adopted for the large vessels; that procedure took about 20 to 30 min for evacuation.

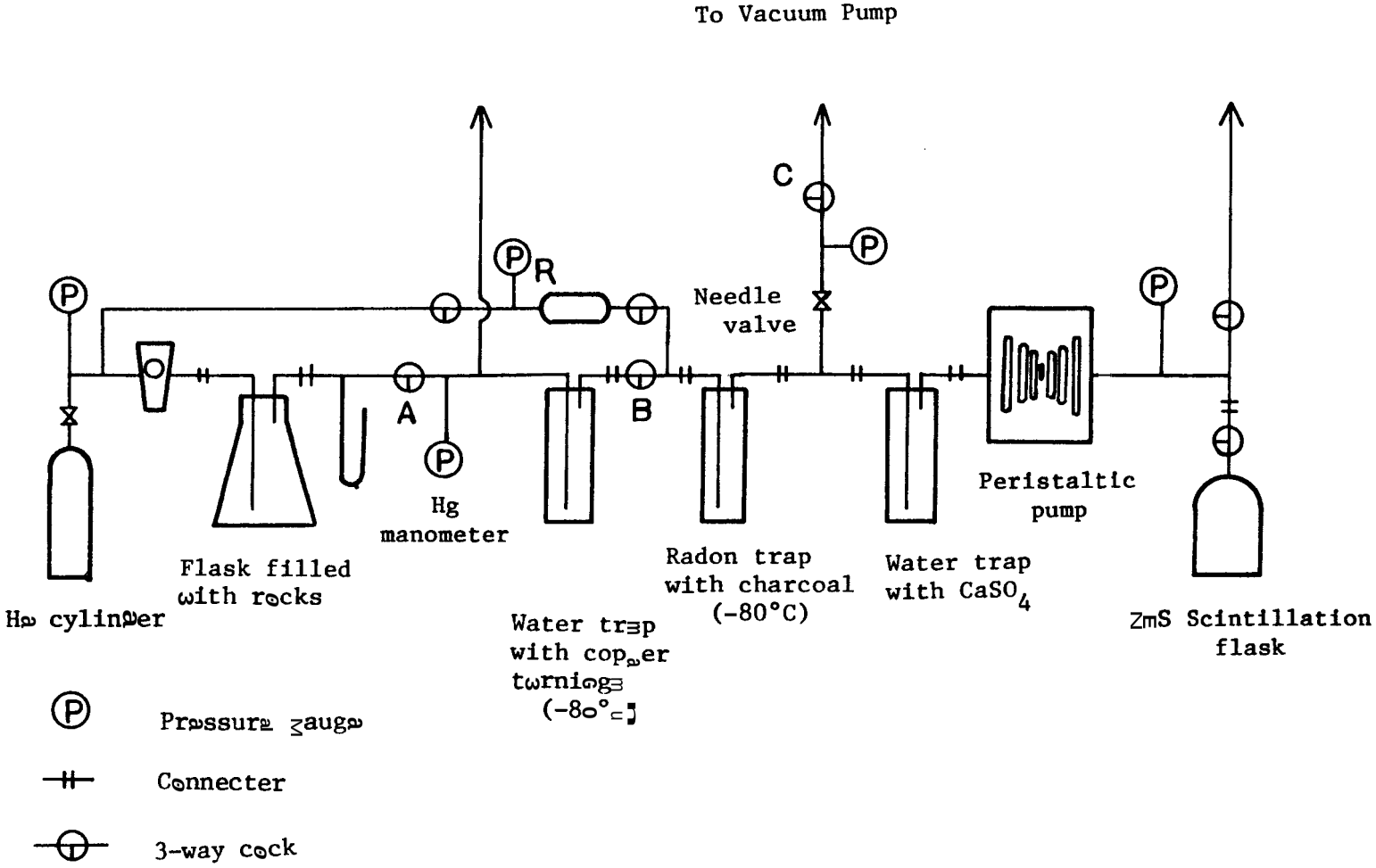

Figure 3-3 Radon extraction system.

In this sweep method, the radon recovery from each vessel was not measured directly. The total recovery efficiency, η, was

$$\eta = 1 - (1 - \varepsilon)^p \qquad (3\text{-}2)$$

where

p = ratio of the total amount of carrier gas used to void space in the vessel; and

E = evacuation efficiency of the system.

As p is about **4** and E is at least 80%, η is almost 100%, barring significant radon adsorption on rock and vessel surfaces.

3.6 RADON MEASUREMENT

Extraction of radon gas adsorbed on activated charcoal was carried out by the method given by Stoker **(1974).** The radon isolation system shown in Fig. 3-3 consisted of a cooled charcoal-adsorption trap system for radon extraction and a ZnS scintillation flask (Lucas, **1964)** for radon measurement. The Lucas flask, which has an effective volume of **100** ml is a reliable alpha-scintillation counter flask containing ZnS on the walls.

The radon gas which was selectively adsorbed on 20 g gas-adsorptive-grade charcoal, *7-14* mesh in size and made from coconut shells, was heated to **400°C** by a metallic-film heating element painted on the glass trap. A measured aliquot of helium gas was let into the trap from the helium reservoir R (Fig. **3-3).** The desorbed radon was transferred into an evacuated scintillation flask by the peristaltic pump. When the pressure in the charcoal trap was reduced to about **10** torr, another aliquot of helium gas was introduced to the trap and transferred to the flask. This flush process was repeated until the flask was filled with radon and carrier gases to a pressure of **1** atm.

Stoker **(1974)** reported that each flush removes about 80% of the He carrier gas remaining in the adsorption trap and final water-vapor-trap portion of the extraction system. About **99%** of the radon is transferred to the outlet side of the system, and the overall volumetric transfer efficiency of the system is about **91%.** The counting efficiency of the scintillation detector was **89%,** and thus the overall system efficiency is calculated to be about 80%.

In this study the overall efficiency of the system, including the counting efficiency for each flask, was determined by using an NBS radium-standard solution. The measured efficiency was between 58% and 61%. This reduced efficiency of the system might be due to prior damage to the scintillation flasks.

3.7 RADIUM ANALYSIS

During the operations of crushing and sieving the rock samples into the various size ranges, special attention was paid to avoiding mineral segregation due to differences in grain size, specific gravity, and hardness scale of each mineral. This was necessary to ensure that radium was retained in constant relative distribution in each particle size range.

To measure the extent of radium content in each size range, radium analysis by the emanation method was carried out. Four different particle sizes (4.00-1.40, 1.40-0.425, 0.425-0.125, and < 0.125 mm) were ground by a disc crusher to obtain uniform samples corresponding to less than 0.075 mm. The analysis was adopted from Johnson and Maxwell (1981), in which 30 g of each sample was fused with 150 g molten sodium hydroxide at 600°C for an hour and dissolved into 1.2 ℓ of water. The solid-suspended solutions were sealed tightly in the same type of flasks used in the room-temperature experiments, and radon was measured after an ll-day buildup. The total radium content was calculated from the radon data.

3.8 MEASUREMENT STATISTICS

3.8.1 Distribution of Sample Means

In view of the limited number of samples that could be run during this work, special attention was given to the accuracy and reproducibility of the data.

In general, the mean of a set of replicate samples, $\bar{v}$, is given by

$$\bar{v} = \frac{\sum_{i=1}^{n} v_i}{n} \qquad (3\text{-}3)$$

where

v_i = value of the i^{th} sample;

n = number of samples.

The variance s^2 is expressed by

$$s^2 = \left[\sum_{i=1}^{n} \frac{(v_i - \bar{v})^2}{n} \right] \qquad (3\text{-}4)$$

In this study, each data value was obtained in triplicate wherever possible. The results are reported as the mean value given by

$$\bar{v} = \frac{\sum_{i=1}^{3} v_i}{3} \qquad (3\text{-}5)$$

and the standard deviation by

$$S = \left[\sum_{i=1}^{3} \frac{(v_i - \bar{v})^2}{3} \right]^{1/2} \qquad (3\text{-}6)$$

The magnitude of the standard deviation for each data point is shown by the error bar.

3.8.2 Sample Variance

Since we can assume that a set of repetitive data will follow the Gaussian distribution, statistical parameters can be estimated. The variance of each sample, s^2, distinguished from the population variance, S^2, can be calculated about its own mean by the following equation:

$$s^2 = \frac{\sum_{i=1}^{n} (v_i - \bar{v})^2}{n - 1} \qquad (3\text{-}7)$$

This sample variance may be the best unbiased sample estimator of the population variance.

In previous studies by Stoker (1974), Warren (1980), and Macias-Chapa (1981), the overall error in independent analyses was reviewed. According to the rules (Beers, 1962) for combining errors of sums and differences of measured independent quantities, the absolute standard deviation is equal to the square root of the sum of the squares of the absolute standard deviations of the measured quantities.

The radon concentration is calculated from the following equation:

$$[Rn] = \frac{SF \cdot RC \cdot F}{M}\left[1 - \exp\left(\frac{t \cdot \ln 2}{T_{1/2}}\right)\right] \qquad (3\text{-}8)$$

where

[Rn] = calculated radon concentration (pCi/kg)

SF = sample fraction

RC = measured radon activity (pCi)

F = collection efficiency

M = mass of rocks (kg)

$T_{1/2}$ = radon half life (day)

t = radon buildup time (day).

The overall error of the radon measurement is given by

$$\left[\frac{\Delta Rn}{Rn}\right]^2 = \left[\frac{\Delta SF}{SF}\right]^2 + \left[\frac{\Delta RC}{RC}\right]^2 + \left[\frac{\Delta F}{F}\right]^2 + \left[\frac{\Delta M}{M}\right]^2 + \left[\frac{\Delta T_{1/2}}{T_{1/2}}\right]^2 + \left[\frac{\Delta t}{t}\right]^2 \qquad (3\text{-}9)$$

Equation 3-9 may now be written as

$$S^2_{Rn} = S^2_{SF} + S^2_{RC} + S^2_F + S^2_M + S^2_{T_{1/2}} + S^2_t \qquad (3\text{-}10)$$

where S^2 shows the variance of each component.

CHAPTER 4

RESULTS

The experimental program resulted in a set of data on four major' aspects affecting radon emanation: annealing, rock size, buildup, and moisture content. Two supplemental experiments were carried out on microscopic observations and radium analysis. The results were classified into four general sections: room-temperature data, elevated-temperature data, microscopic observations and radium analyses. For each data set, an analysis of the data reliability was made.

4.1 ROOM-TEMPERATURE DATA

Annealing and rock size tests were carried out at room temperature. The data are given as emanation power, EP (%), expressed as the radioactivity ratio of radon to radium, at a buildup time of t = 30 days. The room temperature was in the range of 20° to 23°C during the entire experimental period.

4.1.1 Annealing Tests

The effects of annealing on emanation power was examined with the original untreated rock and three rock samples, heat-treated at 120°, 300°, and 500°C. Data for the runs at 1 atm with dry nitrogen and water as the pore fluid are shown in Table 4-1. In these runs, the radon analyses were carried out after a 30-day buildup period to achieve radioactive equilibrium between radium and radon. The values for EP (%)

Table 4.1

Emanation Power of Samples Heat-Treated at Different Temperatures, Run at Room Temperature

	Temperature of Heat Treatment (°C)			
	Unheated	120	300	500
EP in N_2 (%)	***10.7*** ± 2.5	***4.7 ± 0.7***	***4.1*** ± 0.6	2.1 ± 0.5
Coeff. Var. (X)	4.3	14.9	14.9	23.8
EP in Water (%)	7.5 ± 1.5	6.8 ± 1.0	7.2 ± 1.0	6.1 ± 1.0
Coeff. Var. (X)	20.0	14.7	13.9	16.4

consist of the mean value of the triplicate measurements and the root mean square deviation:

$$EP = \bar{v} \pm s \qquad (4\text{-}1)$$

where

$\bar{v}$ = mean value of the triplicated sample run (%);

s = root mean square deviation (%).

The coefficient of variance was calculated from

$$CV = 100 \times \frac{s}{\bar{v}} \qquad (4-2)$$

The observed emanation power for these heat-treated samples ranged between *2.1%* at the highest annealing temperature and *10.7%* for untreated rock in dry nitrogen and between **6.1%** and *7.5%* in water. It was noted that the values of emanation power were higher for water as pore fluid compared to nitrogen for all heat-treated samples. The untreated sample gave the highest emanation power values of *10.7* ± 2.5% and 7.5 ± *1.5%* but with the greater value for nitrogen. Coefficients of variance were between *4.3* and *23.8%* with an average of *15.3%* for the tests.

4.1.2 Rock Size Tests

The effect of rock size on emanation power was examined with a set of experiments using various sizes of graywacke sandstone. Samples were prepared in fine size ranges: *12.4* ± 0.2 (original size), 9.5–8.0, *4.0–1.4, 0.420–0.125,* and < *0.125* mm, with a mean rock size of *12.4, 8.8, 2.7, 0.27,* and *0.03* mm, respectively. Samples were dried at 120°C in advance of the runs to eliminate free water. The first experiment was carried out with dry nitrogen as the pore fluid at a pressure of 1 atm. The same samples were used with water as the pore fluid.

Table *4–2* shows the results of these experiments. The range of emanation power varied between *3.4* and *7.5%* with dry nitrogen and between *5.5* and *16.2%* with water. Higher emanation powers were observed for water compared to nitrogen. The highest emanation power was *7.5%* in nitrogen and *16.2%* in water, both occurring with the smallest mean rock size, *0.03* mm.

The range of the coefficient of variance for these runs was between *5.4* and *25.0%.* The average was 16.6%, similar to the value obtained in the annealing tests.

Table 4.2
Emanation Power as a Function of Rock Size at Room Temperture

	Rock Mean Size (mm)				
	12.4	8.8	2.7	0.27	0.03
EP in N_2 (%)	4.7 ± 0.7	3.6 ± 0.9	3.4 ± 0.8	4.2 ± 0.7	7.5 ± 1.3
Coeff. Var. (%)	14.9	25.0	23.5	16.6	17.3
EP in Water (%)	6.8 ± 1.0	5.6 ± 0.3	6.0 ± 0.8	5.5 ± 1.0	16.2 ± 2.8
Coeff. Var. (%)	14.7	5.4	13.3	18.2	17.3

4.2 ELEVATED-TEMPERATURE DATA

Radon buildup and moisture tests were done under elevated temperatures of 150 to 300°C in the heavy-duty oven, except for the radon buildup calibration using the radium standard solution, which was done at room temperature. The results of this calibration test are given in Section 4.2.1.

4.2.1 Radon Buildup Tests

Calibration of the system was achieved with the buildup of radon from a NBS standard solution of radium containing 80 pCi in 500-mℓ solution, carried out at room temperature. Table 4-3 shows the radon buildup data at measurement times of 3, 8, 11, and 29 days. The radioactivity values are given in dpm, corrected for the flask counting efficiency. The fractional buildup in the table are given as experimental and theoretical values. Experimental fractional buildup is defined as the ratio of the measured radioactivity at a given buildup time, t, to that at the longest buildup time. Theoretical fractional buildup is calculated from $1 - \exp(-0.181\ t)$. Since the reliability of radon measurements is a function of several parameters--sample fraction, measured radon activity, collection efficiency, mass of rock, radon half-life and buildup time, as described in Section 3-8--the calculated experimental fractional buildup values may deviate from the theoretical buildup values.

The buildup data for radon from the original graywacke sandstone at temperatures of 150°, 200°, and 300°C are shown in Tables 4-4 to 4-6, respectively. At each temperature, the radioactivity ratio increases with build-up time. The emanation power at secular equilibrium was 1.22, 1.63, and 2.33% at 150°, 200°, and 300°C, respectively, showing a steady increase with temperature. The coefficient of variance ranged

from 1.1 to 14.6% with an average of 5.6%. This value is much smaller than that for the room-temperature runs.

Table 4-3

Radon Buildup in the NBS Standard Radium Solution at Room Temperature

	Buildup Time (Days)			
	3	8	11	29
Radioactivity of radon (dpm)	47.8	97.8	121.7	140.5
Fractional experimental buildup	0.34	0.70	0.87	1.00
Fractional theoretical buildup	0.42	0.77	0.86	1.00

Table 4-4

Radon Buildup from Graywacke Sandstone at 150°C

	Buildup Time (Days)		
	4	11	31
Radioactivity ratio (%)	0.56 ± 0.03	1.00 f 0.05	1.22 ± 0.50
Coefficient of Variance (%)	5.4	5.0	4.1
Fractional experimental buildup	0.46	0.82	1.00
Fractional theoretical buildup	0.48	0.86	1.00

Table 4-5

Radon Buildup from Graywacke Sandstone at 200°C

	Buildup Time (Days)				
	1	2	5	10	29
Radioactivity ratio (%)	0.24±0.02	0.4f0.06	0.82-1.0.03	1.13f0.05	1.63±0.12
Coeff. Var.(%)	8.3	14.6	3.7	4.4	7.4
Fractional experimental buildup	0.15	0.25	0.50	0.69	1.00
Fractional theoretical buildup	0.17	0.30	0.60	0.84	1.00

Table 4-6

Radon Buildup from Graywacke Sandstone at 300°C

	Buildup Time (Days)			
	1	2	11	33
Radioactivity ratio (X)	0.32 ± 0.01	0.63 ± 0.02	1.80 ± 0.02	2.33 ± 0.21
Coeff. Var. (X)	1.6	3.2	1.1	8.8
Fractional experimental buildup	0.14	0.27	0.77	1.00
Fractional theoretical buildup	0.17	0.30	0.86	1.00

4.2.2 Moisture Tests

To examine the effect of moisture content on emanation power, a set of runs was made with varying partial pressure of water vapor. These runs were conducted with the medium size graywacke sandstone particles of 9.5 to 8.0 mm. The moisture content was expressed as relative vapor pressure; the ratio of partial pressure to the saturated pressure of water vapor at a given temperature. The results are shown in Tables 4-7 to 4-9.

Table 4-7

Radon Emanation Power as a Function of Partial Pressure of Water Vapor at 150°C

	$P_{H_2O}/P_{Sat.}$ at 150°C			
	0.0	0.2	0.4	0.8
EP (%)	3.0 ± 0.3	6.8 ± 0.8	8.8 ± 0.8	9.0 ± 0.4
CV (X)	9.4	1.9	11.2	4.0

Table 4-8

Radon Emanation Power as a Function of Partial Pressure of Water Vapor at 200°C

	$P_{H_2O}/P_{Sat.}$ at 200°C				
	0.0	0.1	0.2	0.4	0.8
EP (X)	4.1 ± 0.3	7.1 ± 0.1	9.0 ± 0.3	10.0 ± 0.5	10.6 ± 0.9
CV (%)	8.3	0.1	3.2	8.5	8.2

Table 4-9

Radon Emanation Power as a Function of Partial Pressure of Water Vapor at 250°C

	$P_{H_2O}/P_{Sat.}$ at 250°C			
	0.0	0.2	0.4	0.8
EP (%)	4.4 ± 0.5	10.1*	11.2*	11.3 ± 0.7
CV (%)	10.5	-	-	6.2

* No repetition.

These runs were carried out for a constant period of 11 days, corresponding to a theoretical fractional buildup of 0.864, and with a small loss in accuracy. The advantage of obtaining a larger set of data offset this loss.

The relative loss of accuracy was estimated by the following equation:

$$s_t = \frac{d\ EP(t)}{dt}$$

$$= k \cdot \exp(-\lambda t)/\lambda \qquad (4-3)$$

where

s_t = the standard deviation for time t;

EP(t) = emanation power as a function of t;

k = a constant.

However, since the standard deviation of EP is defined as the square root of the sum of the variance for each component in Eq. 3-9, the actual error due to the shorter time is not very significant. The observed average coefficient of variance was about 6.7%, comparing favorably with that observed in the room-temperature runs. The data show that emanation power increases steadily over the humidity range of dry to 80% at each temperature as water is added. As in the buildup tests, higher emanation powers were observed for higher temperatures.

4.3 MICROSCOPIC OBSERVATIONS

Table 4-10 shows the mineral distribution of the graywacke sandstone. This sandstone is composed of angular and/or semiangular fragments of quartz, feldspar (~ 60%) and rock fragments (~ 6%) with minor amounts of shale and metabasalt. The grain sizes range from 1 mm to 1/20 mm in diameter with an average of 0.3 mm, as shown in Fig. 4-1.

Table 4-10

Mineral Distribution of Graywacke Sandstone

Minera1	Mode (%)
Quartz	29.4
Feldspar	30.4
Epidote	trace
Apatite	trace
Sphene	trace
Rock fragments (shale metabasalt)	5.8
Cementing materials (clays)	34.4

The cementing materials are composed principally of clay minerals, with a small amount of organic matter, fine-grained quartz and feldspar. The clay minerals were identified as montmorillonite, illite, kaoline-like minerals, and mixed-layer clay and minerals of smectite/chlorite. After annealing, these clay minerals changed in color from dark gray to reddish. Most of the matrix-forming clay minerals in which dehydration of interlayer or interlattice water may occur might be originally fine-grained feldspar, judging from their chemical composition.

4.4 RADIUM ANALYSIS

Table 4-11 shows the data for the analysis of the samples analyzed to determine the radium content in each of the particle size ranges. The data for the four size ranges do not appear to show any significant radium-bearing particle segregation resulting from the grinding operation. The mean value for the radium content was 554 pCi/kg rock with a

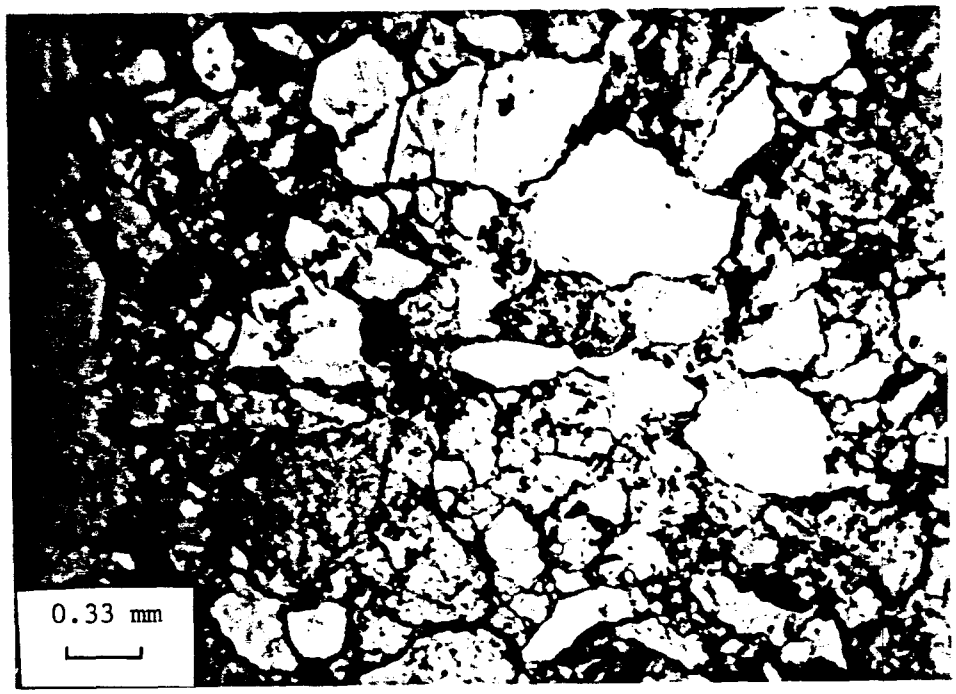

Figure 4-1. Grain size distribution of graywacke sandstone (at 30x magnification).

Table 4-11

Radium Distribution of Crushed Rocks

Particle Size (mm)	Radium (pCi/kg Rock)	EP (%)
4.00-1.40	580.0	95.1
1.40-0.425	589.0	96.5
0.425-0.125	488.4	80.0
< 0.125	556.6	91.2

standard deviation of 46 pCi/kg rock. The corresponding emanation power was 90.7 ± 7.5%. The radium analysis obtained by the emanation method seems to be adequate compared to the direct γ-ray spectrometric analysis value of 610 ± 77 pCi/kg rock determined by Macias-Chapa (1981). To compare the results of this study with results from the previous study, the radium content will be taken as 610 pCi/kg rock.

CHAPTER 5

DISCUSSION OF RESULTS

The experimental data compiled in this program have been examined in several ways. One of these was the determination of mineralogical and petrographical characteristics of the graywacke sandstone by microscopic observation. These data assisted in the evaluation of the effect of heat treatment on the change in radon emanation. Evaluation was made on the effect of rock size on emanation power. The relative importance of recoil escape and diffusion release processes was evaluated based on the experimental results and theoretical expectations.

5.1 ANNEALING EFFECT

5.1.1 Change of Emanation Power in Annealing Tests

Figure 5-1 shows the relation between emanation power and heat-treatment temperature, for the experiments run at room temperature with dry nitrogen and water as the pore fluid. The solid curve shows the data for water and the dashed curve for nitrogen. The emanation-power values shown for room temperature are for the original rock without heat treatment.

The data for dry nitrogen show that the emanation power for the original rock is much higher compared to the heat-treated samples, although the standard deviation of the mean value is also large. The observed change in emanation power over the temperature range from 120" to 300°C was small but increased significantly beyond 300°C.

The change in emanation power for the original rock at a mean value 10.7% to that for the 500°C-heated sample at a mean value of 2.1% corresponds to an 80% reduction in emanation power. This is a relatively large reduction in emanation power and supports the observation of the annealing effect reported by Barretto (1974). A similar magnitude in reduction should be expected for water as the pore fluid. The data for water shown in Fig. 5-2 does show a reduction of emanation power with heat-treatment temperature, but the magnitude is considerably smaller than for nitrogen. The straight line for the water data was calculated by least square regression analysis of the four data points. The

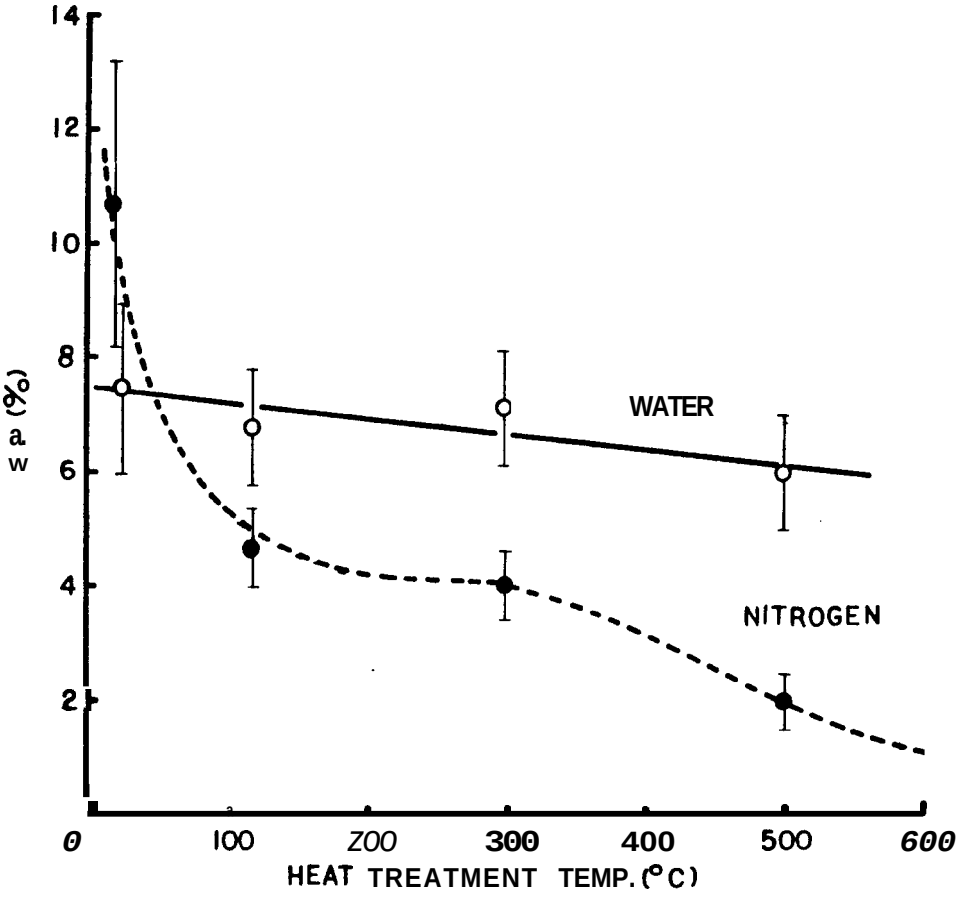

Figure 5-1. Annealing effect on emanation power at room temperature for water and nitrogen as pore fluids.

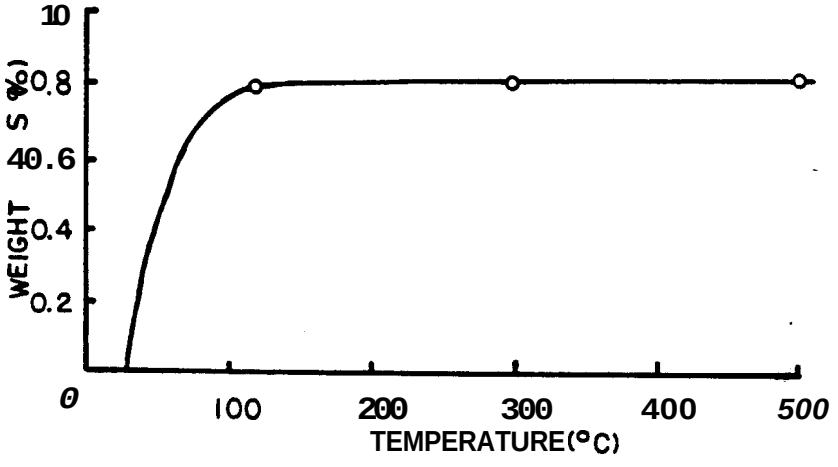

Figure 5-2. Weight loss of graywacke sandstone with heat-treatment temperature.

overall reduction in emanation power from room temparature to 500°C is only about 20% for water, compared to 80% for dry nitrogen.

These two observations are considered as inconsistent results. Compared to the observed reduction for water, it is difficult to understand the large reduction in emanation power in dry nitrogen as being due solely to an annealing effect in the heat treated samples. On the other hand, it is known that moisture in a rock matrix can play an important role in radon emanation (e.g., Tanner, 1978; Rogers et al., 1980). The recoil range of radon varies by medium, in water it is 1×10^{-5} cm, which is about three times longer than that in glass and two orders of magnitude shorter than in air (Tanner, 1964). Water present in rock interstices and pores can absorb the kinetic energy of recoil radon and stop it in the pore space, while in the absence of water some of the recoil-liberated atoms can penetrate into nearby rock and be lost to emanation power. Therefore it is possible that the observed emanation reduction with extended heat treatment is due to elimination of adsorbed water from the rock pores.

Figure 5-2 shows the weight-loss data of the original rocks with heat-treatment temperature. At a heat-treatment temperature of 120°C, it appears that most of the free water was eliminated. The free water consisted of more than 95% of the total water loss, corresponding to 0.83% of the total rock weight.

The data for the heat-treatment experiments suggest that the annealing effect on radon emanation may be minor for the graywacke sandstone used in this study. The observed reduction may he due to the water adsorbed on the rock surface. This possibility is discussed further in evaluation of the moisture effect on radon emanation power.

5.1.2 Radium Source in the Graywacke Sandstone

From microscopic observation, the graywacke sandstone examined in this study was mostly formed by the felsic minerals and cementing materials listed in Table 4-10, but some mafic minerals such as biotite, magnetite, hornblende and augite were also observed.

Among the rarer minerals which Barretto (1974) noted may be important sources of radon, the microscopic examination showed sphene, apatite, allanite and epidote, the total amount of which was less than

1 mole%. Figure **5–3** shows some of these minerals. Other possible minerals containing uranium commonly found in sandstones and granites are zircon, monazite, xenotime and glauconite. Granites and granite pegmatite are considered to be predominant source materials of graywacke sandstone in Great Valley Sequences. None of them were observed in the thin-section samples.

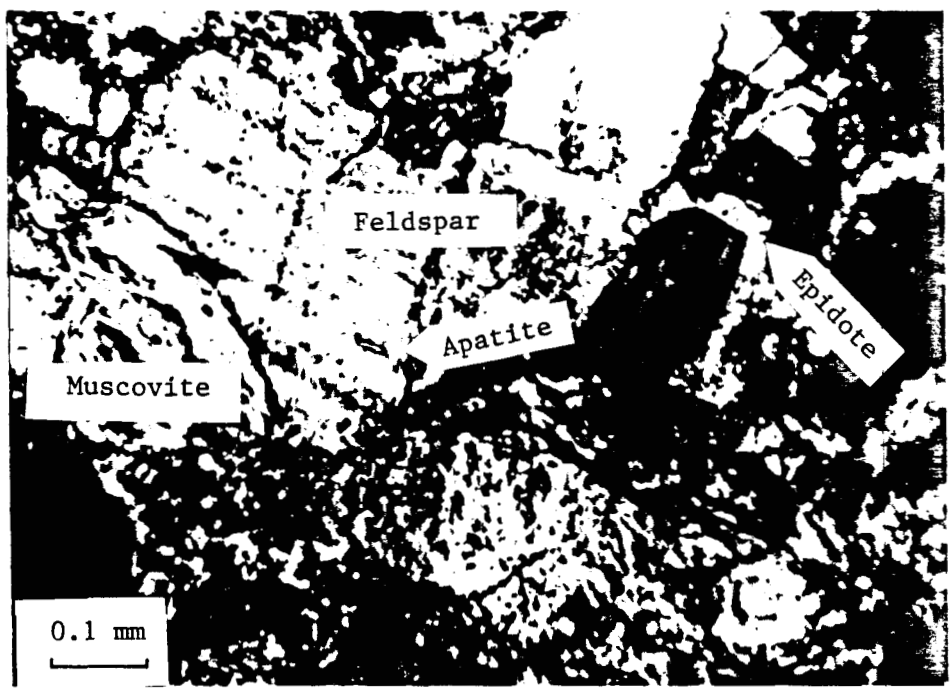

Figure 5-3. Possible uranium-bearing and feldspar minerals in graywacke sandstone (at 120x magnification).

The cementing materials (~ *34%)* were composed principally of clay minerals; chlorite, montmorillonite, illite, kaoline-like minerals, and mixed layer clay and minerals of smectite/chlorite. These clay minerals have a high cation exchange capacity (Bahn et al., 1979). Thus they may be very important as radium-bearing minerals, but were not measured in this study.

During annealing, the graywacke sandstone changed in color from dark gray to reddish, possibly caused by oxidation. Some clay minerals showed thermal change and decomposition, but sphene, apatite, allamite and epidote were microscopically stable up to 500°C. It is possible to attribute some of the mineralogical changes in the sandstone to a

significant effect on emanation power, but quantitative estimate would be very difficult.

5.2 ROCK SIZE EFFECT

5.2.1 Change of Emanation Power

The results for the experiments examining the dependence of emanation power on rock size are shown in Fig. 5-4. The solid curve shows the data for water and the dashed line the data for dry nitrogen as the pore fluid. The nitrogen data were obtained with samples that were heated for two days at 120°C to eliminate free water. It was noted in Table 3-4 that the graywacke sandstone examined in this study has a porosity of 4.9% and a specific surface area of 2.8 m^2/g. These values suggest that the rock should be considered as a porous material and not as solid particles.

The emanation power from rocks of particle-size diameter greater than 300 μm appears to be almost constant with particle size, but increases steeply in rocks of diameter less than 300 μm. The emanation power of the original rock was somewhat higher than the ground rocks. This may be due to the difference in rock shape; the original rock has a thin and elliptical shape while the ground particles can be assumed to be spherical. The characteristic dependence of emanation curve on particle size has the same shape for both fluids, but the values for water are significantly higher than for nitrogen.

The pore size distribution was not determined in this study. Its relationship to specific surface area cannot be determined. However, it seems reasonable to relate grain size and specific surface area from the microscopic observations. The optical pictures of the graywacke sandstone showed a variety of grain sizes, but most of them were in the range from 1 to 1/20 mm. The observed sizes of sphene, apatite and allanite, which might be important as radium-bearing minerals, were 0.4-0.05, 0.01-0.005, and 0.1-0.04 mm, respectively, well within the general range of grain sizes.

In porous materials, if a particle size is much larger than a grain size, e.g. a pore size, the surface area of the particle can be small compared to its inner surface area. Under this condition, the specific

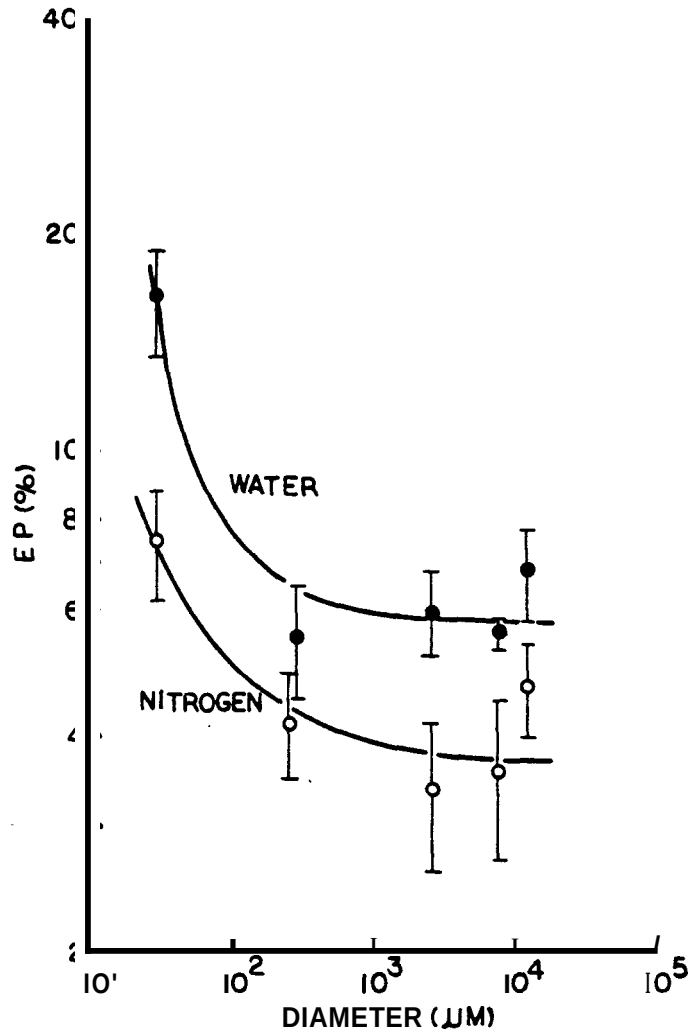

Figure 5-4. Rock size effect on emanation power at room temperature for water and nitrogen as pore fluids.

surface area of a particle does not depend on its size. If this is true for the particles larger than 300 μm, the data given in Fig. *5-4* may reflect a constant inner surface area. However, as the particle size decreases to the value of an average grain size, new surface area can be created by crushing and the specific surface area of a particle can increase significantly. For very small particles, the specific surface area may become inversely proportional to the diameter. The data in Fig. *5-4* may suggest that the threshold diameter for particles approaching grain size is of the order of 300 μm.

Andrews and Wood (1972) reported that a linear relationship cannot be applied to cemented sandstones because of their nonhomogeneity. Cementing materials can also be an important source of radium in graywacke sandstone. However, the optical examination of the samples does not provide information about these minerals as a radon source. Therefore, the contribution of cementing materials (e.g. clays) to radon emanation is not sufficiently known.

In the rock size experiments, water as a pore fluid resulted in higher emanation power than dry nitrogen. Water in pore space can absorb more radon recoil energy than a gas, and thus stop more radon atoms even though radon diffusion in water is much slower than in gas.

The slopes in the fine-particle region, given by log EP(%)/ log d(μm), are about -1.5 in water and -1.0 in nitrogen. From these values, rock size dependence on emanation power is inversely proportional to $d^{1.5}$ and d for water and nitrogen in that size region respectively. By extrapolation of the curve for water, 100% emanation power in water occurs at a particle diameter of 1 μm. For nitrogen much finer particles ($\sim 10^{-2}$ μm) are needed to yield 100% emanation power. The difference may imply that some radon atoms are lost by penetrating into neighbor rocks in nitrogen as the pore fluid.

5.2.2 Segregation of Minerals

The data in Table 5-1 shows an average radium content of 554 pCi/kg rock, with a sample standard deviation 45 pCi/kg rock and a coefficient of variance of 8.2%. This radium content agrees within 90% of the value of 613 ± 77 pCi/kg rock reported by Macias-Chapa (1981). The corresponding values for the emanation power based on this radium analysis' data were 95.1%, 96.5%, 80.0% and 91.2% in order of decreasing sample size. The average value of 90.7% for the emanation power for all samples is lower by 4% because of the relatively low value of 80.8% EP in the size range 0.425 to 0.125 mm, but the overall agreement is generally quite satisfactory.

The radium content of the smallest sample does not show a significantly high value. The high emanation power observed in Fig. 5-4 cannot be explained by selective segregation of radium-bearing minerals in the

Table 5-1

Statistics of Radium Distribution of Crushed Rocks

Mean radium content (pCi/kg rock)	554
Sample standard deviation (pCi/kg rock)	45
Coefficient of variance (%)	8.2

fine-particle sample. The high value of the emanation power is thus due to the rock size effect.

5.3 DIFFUSION PROCESS

5.3.1 Diffusion Coefficient of Radon

On the assumption that the contribution to emanation power by direct recoil is small, the diffusion coefficient of radon from graywacke sandstone can be estimated from emanation power data at various temperatures. Table 5-2 gives a summary of the various conditions of rock size and moisture content for the emanation power measurements. Condition I involves the original size of the graywacke sandstone tested under vacuum at temperatures of 150°, 200° and 300°C. Condition II to V involve the crushed rock of 8.8 mm mean-particle size at temperatures of 150°, 200° and 250°C and at relative vapor pressures of 0.0, 0.2, 0.4 and 0.8.

Figure 5-5 shows the relationship of emanation power to reciprocal temperature for varying rock size and relative vapor pressure in the reservoir. Each curve was determined by least-square regression analysis of three data points. The slope of each curve is expressed (from Eq. 2-39) as $-Q_E/R$ and the y-intercept as $\ln kA'$. Values of A and Q_Γ can be obtained (from Eq. 2-38) from the value of the slope and the y-intercept for each regression curve. From Eq. 2-36, the diffusion coefficient for radon is determined at a given temperature. Table 5-3 lists the y-intercept and the slope of each curve in Fig. 5-5. The results of the calculations of the diffusion coefficient for radon are listed in Table 5-4.

Table 5-2

Various Conditions of Emanation Power Measurement

Condition #	Rock Size (mm) Range	Mean	Moisture (RVP at 150-300°C)
I	Original	12.4	0.0 (vacuum)
II	9.5–8.0	8.8	0.0 (vacuum)
III	9.5–8.0	8.8	0.2
IV	9.5-8 .0	8.8	0.4
V	9.5–8.0	8.8	0.4

* See Table 3-1.

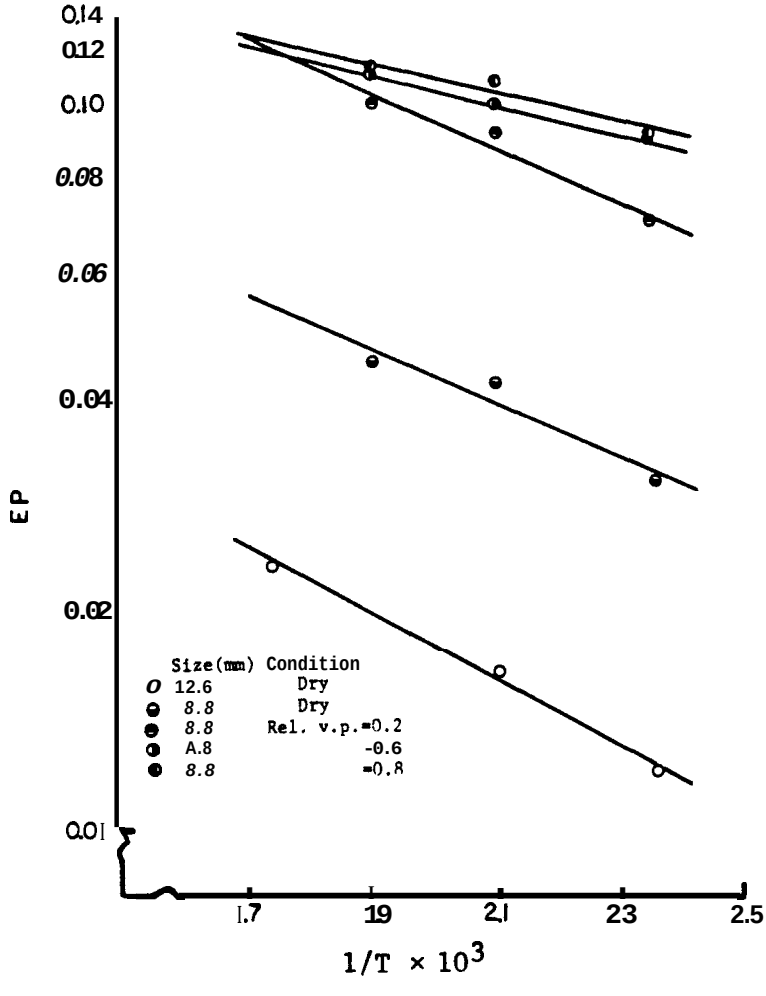

Figure 5-5. Relationship of emanation power to reciprocal temperature for varying rock size and relative vapor pressure in the reservoir.

Table 5-3

Linear Regression Curves of Emanation Power
ln EP vs Temperature 1/T

Condition #	y-Intercept (ln kA')	Slope ($-Q_E/R$)
I	-1.938	-1040.0
II	-1.437	- 863.1
III	-0.581	- 883.5
IV	-1.174	- 532.2
V	-1.190	- 510.3

Table 5-4

Diffusion Coefficients of Radon under Various Humidity Conditions

	Diffusion Coefficient (10^{-12} cm^2/s)				
Condition #	20°C	150°C	200°C	250°C	300°C
I	1.54	13.6	22.9	34.9	49.4
II	14.0	85.5	132	187	249
III	33.9	217	337	481	643
IV	114	348	455	564	673
V	128	374	483	593	703

Further discussion is needed concerning the assumption that emanation power is primarily due to diffusion with little contribution by direct-recoil in a large particle size range. Since water adsorbed on the rock surface may have a significant effect on the number of recoil radon atoms that stop in the pore space, a high humid environment should yield a higher emanation power compared to a dry environment. One would expect the diffusion coefficient to increase with increasing humidity as noted for Conditions III to V in Table 5-4. However, the large diffusion coefficient observed for the high humidity samples does not

necessarily imply a high diffusivity of radon under dry-steam conditions; it is more likely attributed to an increase of radon atoms stopping in the pore space. In fact, Tanner (1964a) noted that increased moisture in a porous medium can cause a reduction of the diffusion coefficient of radon. On the basis that the contribution of recoil atoms to the observed emanation power is significant, the evaluation of the diffusion coefficient is more difficult. The diffusion coefficient may not simply be compared under different moisture conditions alone.

From the value of the slopes in Fig. 5-5 and the relation between Q_E and Q_D in Eq. 2-38, we can calculate the activation energy of radon diffusion, Q_E, which is temperature dependent. The calculated activation energies of 7.35, 4.43 and 4.24 KJ/mol for Conditions III, IV and V, respectively, show a decrease with increasing amounts of added water. The data indicate that diffusion is less dependent on temperature under wet conditions.

According to diffusion theory (Shewman, 1963), the diffusion coefficient of an atom is independent of size and shape in a homogeneous matrix. On the other hand, emanation power is a function of matrix size and shape, as noted in Section 2-2-2. To establish a mathematical model for radon emanation, Flügge and Zimens (1939) assumed a spherical particle shape. Their assumption is probably satisfactory for the crushed samples in this study, but it is known that the original rock has a thin and elliptical shape; the mean dimensions were given in Table 3-1. In the dry environment of Conditions I and II, the crushed rock had a diffusion coefficient 5 to 10 times greater than the original rock in Table 5-4. The difference in shape may be partially responsible for the inconsistency in the values of the diffusion coefficient under the two conditions. Other reasons may be more important.

In the simple mathematical expression of Eq. 2-29, which is valid for large particles, the relation between particle radius, diffusion coefficient and emanation power has two degrees of freedom. Thus the third parameter is determined if two of the above parameters are known. Figure 5-6 shows two curves of the relation between log EP and log D for two particle sizes; 8.8 mm and 12.4 mm. Interpolating values of emanation power from these curves, the diffusion coefficient corresponding to

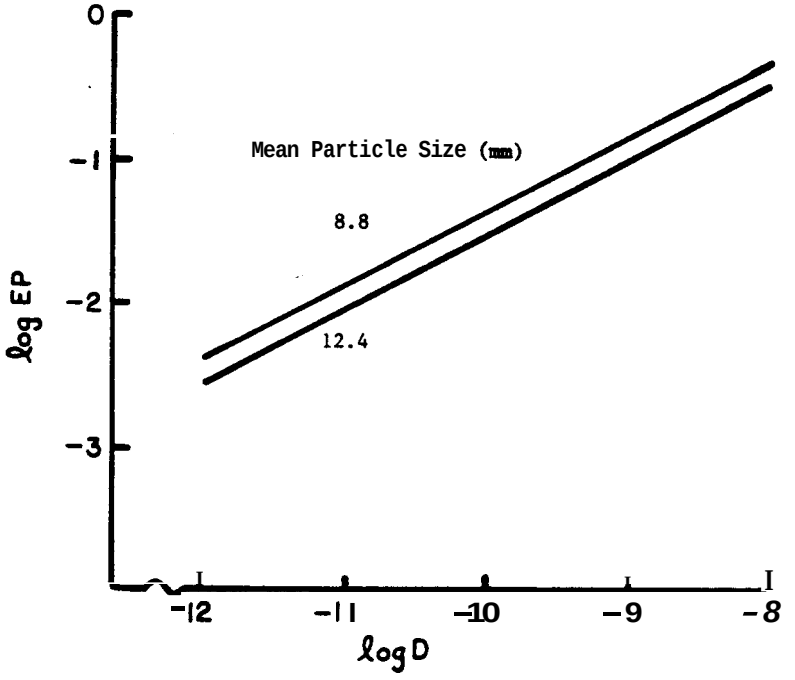

Figure *5-6.* Relationship of emanation power and diffusion coefficient (log-log scale).

the emanation power can be estimated. Table *5-5* lists a summary of the results. The diffusion coefficients given in Fig. *5-6* are in good agreement with those from the experiments in this study. These are listed in Table *5-4.* The calculated diffusion coefficients from both the experimental data and from the mathematical model of Eq. *2-29* are based on the assumption that the particles are large enough to neglect the effect of direct-recoil radon.

Table *5-5*

Diffusion Coefficients Given from Eq. *2-29*

	Diffusion Coefficient (10^{-12} cm2/s)			
Condition #	*150°C*	*200°C*	*250°C*	300°C
I	*20.0*	*31.2*	-	*39.8*
II	*40.4*	*75.0*	*86.9*	-
III	*207*	*337*	*457*	-
IV	*347*	*448*	*562*	-
V	*398*	*504*	*572*	-

The apparent agreement may also be due to the effect of humidity. Under humid conditions, recoil atoms of radon from grains of radium-bearing minerals may be more efficiently stopped in the pore space, from which radon can easily diffuse. The data in Tables ***5-4*** and ***5-5*** show that for the water-added conditions, the diffusion coefficient is one or two orders of magnitude larger than for dry conditions, indicating a difficulty in the assumption concerning the humidity conditions.

From Eq. **2-30** it is noted that emanation power is inversely proportional to particle size in both the diffusion and recoil processes. In fine particles (e.g., < **1** μm) the recoil process may be the controlling' process because of geometric factors and a short diffusion path length. However, for larger particles both processes may be important, but the number of recoil radon atoms per unit pore volume may not depend on rock size, if the particle size is large compared to its grain size. Nevertheless, emanation power should be inversely proportional to rock size in the diffusion process. Thus, the relationship of emanation power to rock size in large particles (see Fig. ***5-4)*** cannot be explained solely as a diffusion process. This observation requires further consideration.

The data showed a significant difference in emanation power for the two original size samples; one which was loaded in a large steel vessel and another in a glass flask. Emanation power from the large vessel run at higher temperature was only one-fourth as high as that from the glass flask run at room temperature. The inconsistency may be due to the fact that the rocks in the large vessel were dried at **300°C** for several, months to eliminate water in the vessel before running the experiments., On the other hand, rocks in the flask were heated for two days at **120°C** and cooled to room temperature in open air. Thus, the racks in the flask may have contained a significant amount of adsorbed water.

From these considerations, it may be concluded that these data do not support the radon emanation model proposed by Flügge and Zimens **(1939)** for porous rocks. The effect of recoil radon in porous rocks may not be neglected and the diffusion process may not be the sole control of the radon emanation in large, porous grains. The data indicates that the water adsorbed on the rock surface results in significant contribution of recoil radon atoms to the pore space.

5.3.2 Time Dependence of Emanation Power

Previous discussions were based on occurrence of radon emanation under steady-state conditions; i.e., emanation power was independent of time. To evaluate the validity of this assumption, the time dependence of emanation power as a function of rock size was evaluated. Diffusion coefficients were computed from the non-steady-state equation of emanation power given by Kapustin and Zaborenko (1974). Figure 5-7 shows the results of the calculations of emanation power for particles with a 1000 μm radius as a function of time. The time dependence decreases with decreasing diffusion coefficient. For the case of $D = 1.0 \times 10^{-7}$ cm^2/sec, the curve indicates that steady-state conditions are established after 7 or 8 days. For smaller values of the diffusion coefficient and larger values of particle size, resulting in smaller emanation power, steady-state conditions were established in less than one day. In this study, the minimum buildup time for radon measurement was one day. Thus all of the radon measurements were done under steady-state conditions.

Figure 5-8 shows the buildup curves for the original size rock run at temperatures of 150°, 200°, and 300°C. These experimental results do not show any non-steady-state effects. From the data in Tables 4-4 through 4-6, the mean deviation of actual from theoretical buildup is -12% for all of the buildup tests. Figure 5-9 shows the theoretical radon buildup curve plotted in relation to the experimental results for the NBS radium standard solution of 80 pCi.

5.3.3 Moisture Effect on Emanation Power

It was noted in Section 5.1.1 that the annealing effect on emanation power is minor in graywacke sandstone. The observed data for the heat-treated rocks could be explained by surface-adsorbed water. Figure 5-10 shows the relation between emanation power and relative vapor pressure at temperatures of 150°, 200°, and 250°C. Addition of about 200-2000 ppm of water to achieve the desired humidity in the rock caused a significant increase in emanation power. The data show that emanation power reaches a saturation value at a relative vapor pressure of 0.4 and does not increase further with increased humidity.

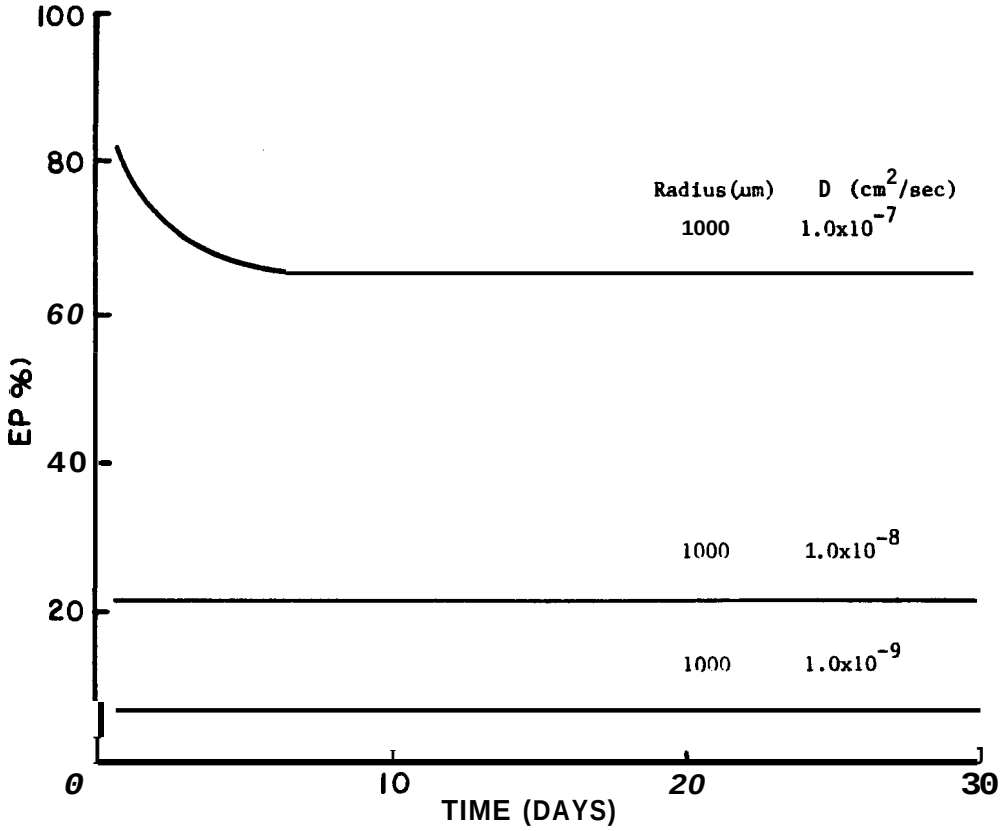

Figure 5-7. Time dependence of emanation power as a function of diffusion coefficient for a mean particle size of 1 mm.

Hsieh (1980) measured water-adsorption isotherms for Berea sandstone at various temperatures between 100° and 200°C. Figure 5-11 shows the water-adsorption isotherm at 172.60°C (from Hsieh, 1980). The water adsorbed on the Berea sandstone was deemed sufficient to cause multilayers of adsorbed water proportional to the relative vapor pressure, independent of temperature. As the amount of surface water increases with increasing humidity (Hsieh, 1980), the observed emanation power increased. The observed increase may be due to the increased efficiency of radon atoms stopping in the pore space. At a relative vapor pressure of 0.4, the water-layer thickness consistent with maximum stopping power for recoil of radon atoms from grains could be established and emanation power would not increase further with an increase of water.

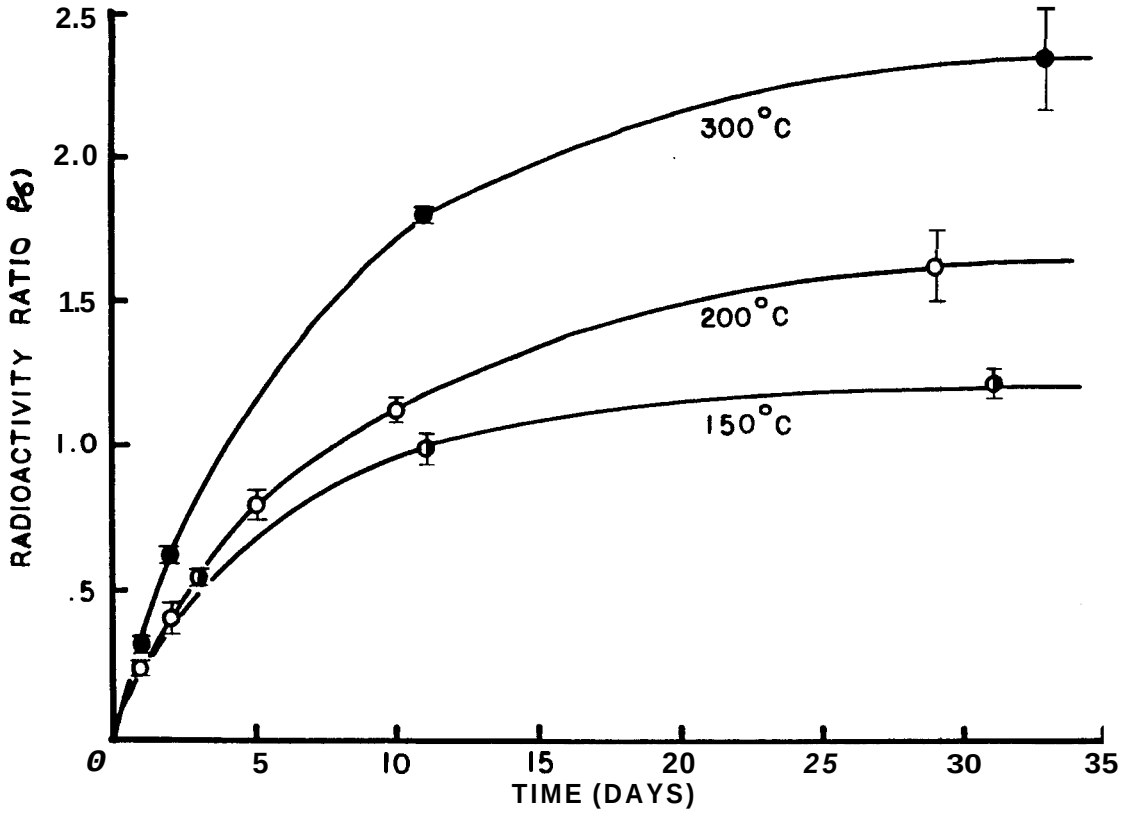

Figure 5-8. Buildup curves of radon as a function of temperature.

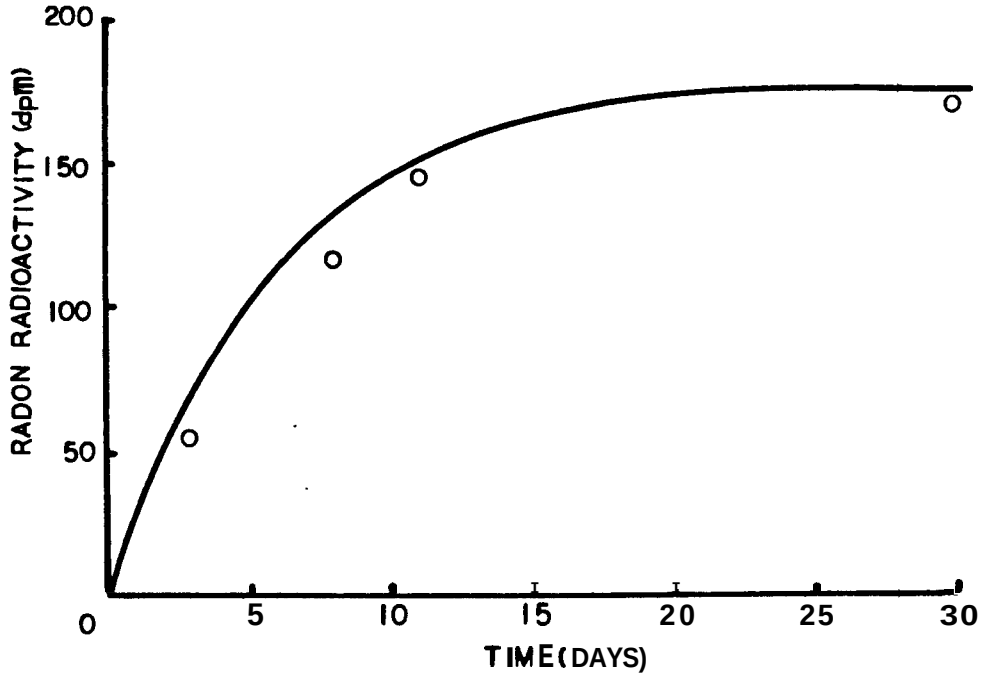

Figure 5-9. Theoretical buildup curve for the NBS radium standard solution in relation to the experimental data.

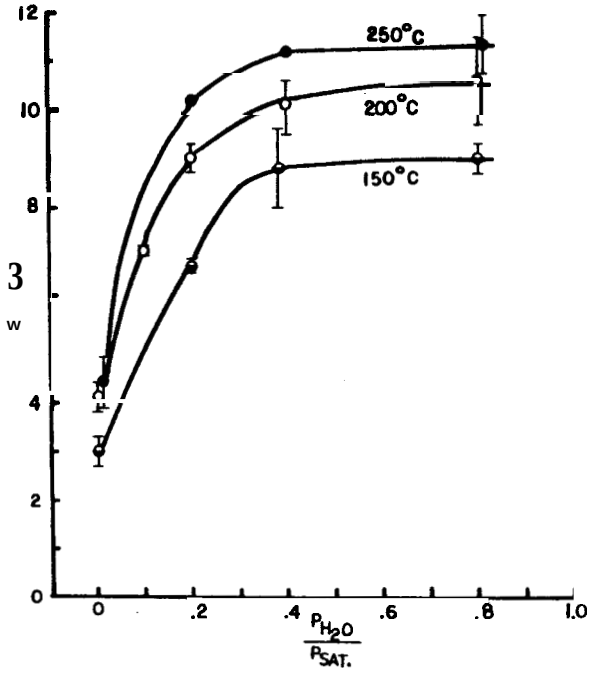

Figure 5-10. Emanation power as a function of relative vapor pressure for various temperatures.

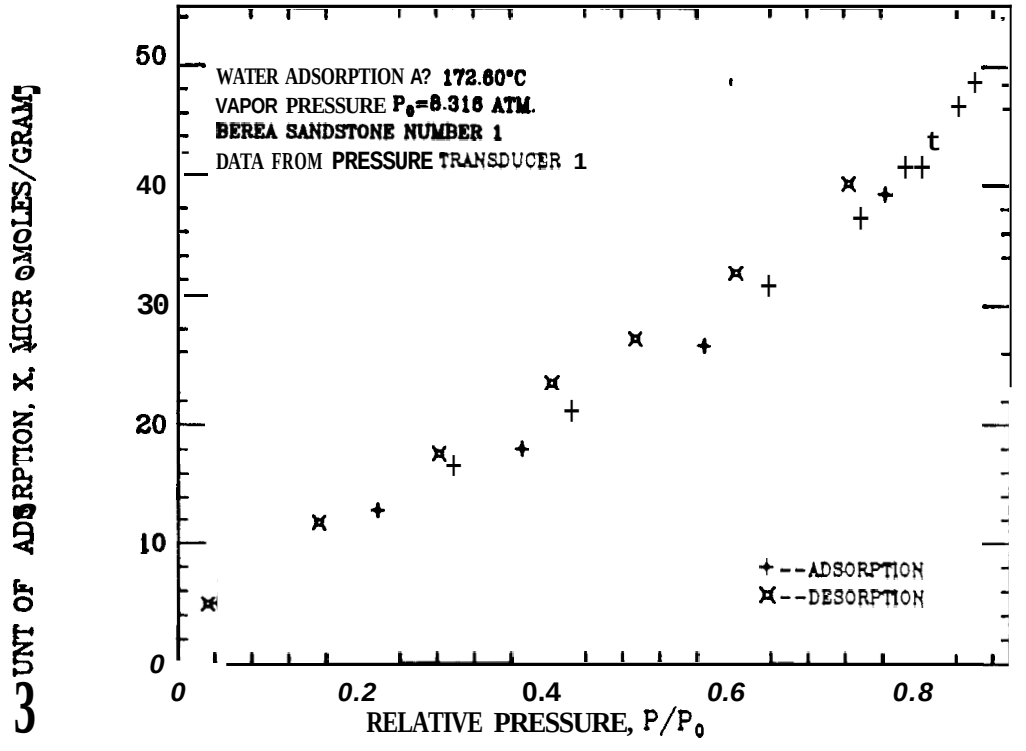

Figure 5-11. Water adsorption isotherm at elevated temperature (from Hsieh, 1980).

5.3.4 Model of Radon Emanation Mechanism from Porous Rock

From the results given in this study, a model of radon emanation mechanism from porous rock is proposed. A schematic diagram of this model is shown in Fig. 5-12. The radon is released from the radium-bearing particle by recoil or diffusion. The direct-recoil radon process becomes insignificant as the particle size becomes much larger than its grain size. The rate of direct-recoil is not very dependent on the physical conditions of temperature, pressure, and water content. The process of recoil within the grain or to the rock pore space depends on the thickness of surface water. The rate of diffusion to the pore space is also dependent on temperature. Thus, for large particles, the direct-recoil of radon can be neglected, and the other two pathways are influenced by the physical conditions. Since the diffusion coefficient in the rock pore space could be about one or two orders of magnitude larger than in a solid grain, radon recoil to the pore space should be the most important process in emanation power from large porous particles.

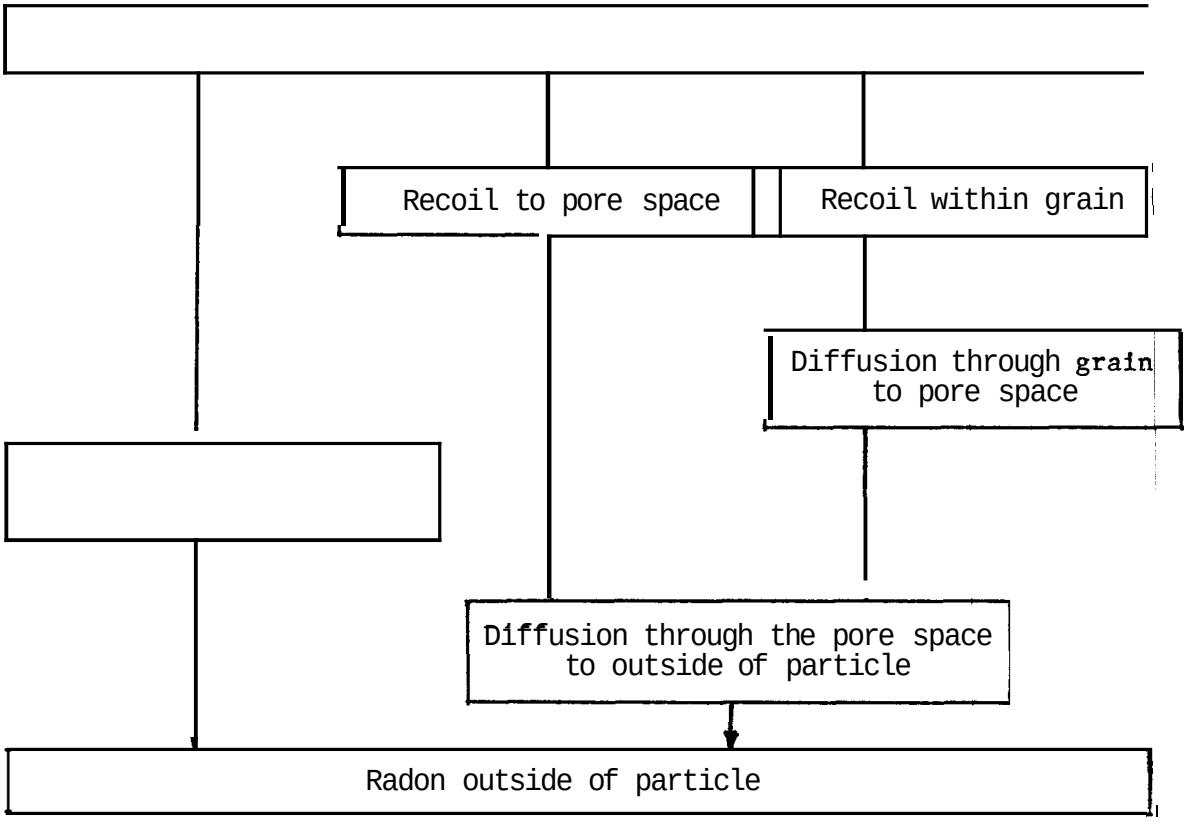

Figure 5-12. Schematic diagram of a radon emanation model far emanation' of radon from porous rock.

CHAPTER 6

CONCLUSIONS AND RECOMMENDATIONS

Investigation was made of three major effects on radon emanation in porous rocks: annealing, rock size, and moisture content. Evaluation was made of two mechanisms of radon emanation to pore fluids: direct recoil and diffusion.

6.1 CONCLUSIONS

6.1.1 Major Effects

Annealing

The annealing effect on graywacke sandstone was expected to cause a reduction of emanation power. The observed effect was small compared to the effect of moisture. Microscopic examination showed that some clay minerals underwent thermal change by the heat treatment. Other minerals, such as sphene, apatite, and epidote, seemed to be thermally stable up to 500°C.

Rock size

Emanation power from finely ground particles of mean diameters less than 300 μm showed a steep increase compared to the larger particle sizes. This observation is interpreted as a contribution to emanation power due mainly to direct-recoil of radon for particles approaching grain size, as new surface area is created by crushing. Emanation power from the larger samples showed less dependence on rock size. For particles of porous rocks large compared to their grain size, the surface area can be much smaller than the inner surface area. In that case, the efficiency for radon emanation would be independent of particle size. For the diffusion process alone, however, the results are not clear because emanation power due to diffusion is expected to be inversely proportional to rock size.

Moisture content

The data showed that water adsorbed on the rock surface plays a significant role in radon emanation. Emanation power increased rapidly with addition of water up to a saturation level at a relative vapor

pressure of 0.4, apparently corresponding to a water-layer thickness effective for stopping radon recoil atoms.

6.1 Emanation Mechanisms

Radon emanation is the result of two processes: recoil and diffusion. For small particles, the recoil of radium source to the pore volume in the particle is an important mechanism. The amount of water retained on the rock surface becomes important, as grain size increases. Diffusion of stopped radon from within a grain to the pore space is another important radon migration process. The number of recoil and diffusion mechanisms in the pore depends not only on physical conditions, such as temperature, pressure, and water content, but also on the particle characteristics such as grain size and porosity. The data indicate that diffusion coefficients of the order of 10^{-10} to 10^{-11} cm^2/sec were consistent with the radon emanation power for the dry samples at mean grain size of 12.4 to 8.8 mm.

6.2 RECOMMENDATIONS

Further study of radon emanation from porous rock will require a detailed mathematical model of the direct recoil and diffusion process. The existing model for solid particles should be extended for porous particles through comparative experiments of radon emanation from a solid rock, such as granite. The results should yield information about radon emanation as a function of rock size and moisture content. Diffusion coefficients obtained for solid particles should be compared to the values obtained for porous particles.

In this study, super-heated conditions were used to examine the effect of water adsorbed on the rock surface in relation to the stopping power of radon atoms. However, under-saturated conditions are much more frequent in most geothermal reservoirs. Extension of the measurements to these conditions would be desirable. A study of emanation power under various water saturations through a known core sample would be useful to observe the effect of fluid movement on radon emanation.

REFERENCES

Adams, J. A. S., and W. M. Lowder, 1964. The Natural Radiation Environment. University of Chicago Press, Chicago.

Andrews, J. N., and D. F. Wood, 1972. "Mechanism of Radon Release in Rock and Matrices and Entry into Ground Water," Trans. Inst. Mining and Metallurgy, B198-209.

Barretto, P. M. C., 1975. "Radon-222 Emanation Characteristics of Rocks and Minerals," International Atomic Energy Agency, IAEA-PL-505/1.

Beers, Y., 1962. Introduction to the Theory of Error. Addison-Wesley Publishing Company, Reading, MA.

Belin, R. E., 1959. "Radon in the New Zealand Geothermal Regions," Geochim. Cosmochim. Acta, 16, 181-191.

Bohn, H. L., B. L. McNeal, and G. A. O'Connor, 1979. Soil Chemistry. John Wiley & Sons, New York.

Clever, H. L., 1979. "Krypton, Xenon and Radon-Gas Solubilities," Solubility Data Series, Vol. 2. Pergamon Press, New York.

Cook, G. A., 1961. Argon, Helium and the Rare Gases; the Elements of the Helium Group. Interscience Publishers, New York.

Crank, J., 1975. The Mathematics of Diffusion. Clarendon Press, Oxford.

D'Amore, F., J. C. Sabroux, and P. Zettwoog, 1978. "Determination of Characteristics of Steam Reservoirs by Radon-222 Measurements in Geothermal Fluids," Paleoph., 117, 253-261.

Faure, G., 1977. Principles of Isotope Geology. John Wiley & Sons, New York.

Flügge, S., and K. E. Zimens, 1939. "Die Bestimmung von Korugrössen und von Diffusionskonstanten aus dem Emanierrermb'gen," (in German), Z. Physik. Chem., B42, 179.

Friedlander, G., J. W. Kennedy, E. S. Macias, and J. M. Miller, 1981. Nuclear and Radiochemistry, 3rd ed. John Wiley & Sons, New York.

Gary, M., R. McAfee, Jr., and C. L. Wolf, 1972. Glossary of Geology. American Geological Institute, Washington, D.C.

Giletti, B. J., and J. Tullis, 1977. "Studies in Diffusion IV: Pressure Dependence of Ar Diffusion in Phlogopite Mica," Earth Planet Sci. Lett., 35, 180-183.

Glasstone, S., K. J. Laidler, and H. Eyving, 1941. Theory of Rate Process. McGraw-Hill Book Co., New York.

Hahn, O., and O. Müller, 1923. "Eine Neue Methode zum Studium der Oberfläche und Oberflächenänderung Feinverteilter Niederschläge," Z. Elektrochem., 29, 189-192.

Hammond, D. E., H. J. Simpson, and G. Mathieu, 1977. "Radon 222 Distribution and Transport Across the Sediment-Water Interface in the Hudson River Estuary," J. Geophys. Res., Sep. 20, 3913-3920.

Heckter, M., 1934. "Radiochemische Oberflichenbestimmung an Glas," Glastech. Ber., 12, 159-172.

Hoogteijling, P. J., G. J. Sizoo, and J. L. Yntema, 1948. "Measurements on the Radon Content of Groundwater," Physica, 14, 73-80.

Hsieh, Chih-Hang, 1980. "Vapor Pressure Lowering in Porous Media," Ph.D. Dissertation, Stanford University, Stanford, CA.

Hunsbedt, A., P. Kruger, and A. L. London, 1975. "A Laboratory Model of Simulated Geothermal Reservoirs," Report SGP-TR-7, Advanced Technology Dept., RANN, National Science Foundation, Grant No. GI-34925, February.

Hyndman, D. W., 1972. Petrology of Igneous and Metamorphic Rocks. McGraw-Hill Book Co., New York.

Johnson, W. M., and J. A. Maxwell, 1981. Rock and Mineral Analysis, 2nd ed. John Wiley & Sons, New York.

Kapustin, O. A., and K. B. Zaborenko, 1974. "Calculation of Degree of Liberation of Radioactive Gases from Solids and Determination of Diffusion Coefficients," translated from Radiokhimiza, 16(5), 611-617.

Kruger, P., C. Cederberg, and L. Semprini, 1978. "Radon Data--Phase I Test LASL Hot Dry Rock Project," Report SGP-TR-27. Stanford Geothermal Project, Stanford University, Stanford, CA.

Kruger, P., A. Stoker, and A. Umaña, 1977. "Radon in Geothermal Reservoir Engineering," Geothermics, 5, 13-19.

Kruger, P., and G. Warren, 1977. "Radon Emanation in Geothermal Steam," Trans. Amer. Nuc. Soc., 26, 125.

Kuroda, K., and Y. Yokoyama, 1949. "On the Equilibrium of the Radioactive Elements in the Hydrosphere, I and II," Bull. Chem. Soc. Japan, 21, 52-63.

Kuroda, K., and Y. Yokoyama, 1948. "On the Equilibrium of the Radioactive Elements in the Hydrosphere, III and IV," Bull. Chem. Soc. Japan, 22, 34-45.

Lambert, G., and P. Bristeau, 1973. "Migration of Radon Atoms Implanted in Crystals by Recoil Energy," J. Physique, Colloque C5, Suppl. to No. 11-12, 34(C5), 137-138.

Lambert, G., P. Bristeau, and G. Polian, 1972. "Evidence of Little Migration of Radon Within Rock Grains," Comptes Rendus Acad. Sci. [Paris], Ser. D., 25(274), 3333-3336.

Lucas, H. F., 1964. "A Fast and Accurate Survey Technique for Both Radon-222 and Radium-226,'' in The Natural Radiation Environment, Adams and Lower, editors. University of Chicago Press, Chicago.

Macias-Chapa, L., L. Semprini, and P. Kruger, 1980. "Radon Emanation and Transect Studies," Report SPE-8990, Society of Petroleum Engineers of AIME.

Macias-Chapa, L., 1981. "Radon Emanation in Geothermal Reservoirs," Engineer's Thesis, Stanford University, Stanford, CA.

Martens, C. S., G. W. Kipphut, and J. V. Klump, 1980. "Sediment-Water Chemical Exchange in the Coastal Zone Traced by in situ Radon-222 Flux Measurements," Science, 208(18 April), 285-288.

Mazor, E., 1962. "Radon and Radium Content of Some Israeli Water Sources and a Hypothesis on Underground Reservoirs of Brines, Oils and Gases in the Rift Valley," Geochim. Cosmochim. Acta, 26, 765-786.

Miholić, S., 1958. "Radioactive Waters from Sediments," Geochim. Cosmochim. Acta, 14, 223-233.

Newton, R., and G. F. Round, 1961. "The Diffusion of Helium Through Sedimentary Rocks," Geochim. Cosmochim. Acta, 22, 106-132.

Parker, S. P., 1982. Encyclopedia of Science & Technology. McGraw-Hill Book Co., New York.

Quet, C., J. Rousseam-violet, and P. Bussier, 1975. "Recoil Emanating Power and Specific Surface Area of Solids Labeled by Radium Recoil Atoms. I. Theory for Single Solid Particles," Radiochem. Radioanal. Letter, 23(5-6), 359.

Reynolds, W. C., 1979. Thermodynamic Properties in SI. Department of Mechanical Engineering, Stanford University, Stanford.

Rogers, A. S., 1958. "Physical Behavior and Geologic Control of Radon in Mountain Streams," U.S.G.S. Bull. 1052-E.

Rogers, V. C., and R. F. Ouermyer, 1980. "Characterization af Uranium Tailings Cover Material for Radon Flux Reduction," NUREG/CR/08, U.S. Nuclear Regulatory Commission, Washington, D.C.

Sakakura, A. Y., C. Lindberg, and H. Faul, 1959. "Equation af Continuity in Geology with Applications to the Transport of Radioactive Gas," U.S. Geol. Survey Bull., I, 1052.

Semprini, L., 1981. "Radon and Ammonia Transects in Geothermal Reservoirs," Engineer's Thesis, Stanford University, Stanford, CA.

Semprini, L., and P. Kruger, 1980. "Radon Transect Analysis in Geothermal Reservoir," Report SPE-8890, Society of Petroleum Engineers of AIME.

Shewman, P. G., 1963. Diffusion in Solids. McGraw-Hill Book Co., New York.

Stanton, R. L., 1972. Ore Petrology. McGraw-Hill Rook Co., New York.

Stoker, A. K., 1974. "Radon Measurements in Geothermal Systems," Engineer's Thesis, Stanford University, Stanford, CA.

Stoker, A. K., and P. Kruger, 1975. "Radon in Geothermal Reservoir," Proc. Second United Nations Symposium on the Development and Use of Geothermal Resources, San Francisco, CA, May 20-29, 1975.

Strong, K. P., and D. M. Levins, 1982. "Effect of Moisture Content on Radon Emanation from Uranium Ore and Tailings," Health Physics, 42(1), 27-32.

Tanner, A. B., 1964a. "Radon Migration in the Ground: A Review," in The Natural Radiation Environment, Adams and Lowder, editors. Symposium Proceedings, Houston TX, April 10-13, 1963. University of Chicago Press, Chicago.

Tanner, A. B., 1964b. "Physical and Chemical Controls on Distribution of Radium-226 and Radon-222 in Ground Water Near Great dalt Lake, Utah," in The Natural Radiation Environment, Adams and Lowder, editors. Symposium Proceedings, Houston TX, April 10-13, 1963. University of Chicago Press, Chicago.

Tanner, A. B., 1978. "Radon Migration in the Ground: A Supplementary Review," Open File Report 78-1050, U.S. Geological Survey.

Wahl, A. C., 1951. "Emanation Methods," Chap. 9 in Radioactivity Applied to Chemistry, A. C. Wahl and N. A. Bonner, eds. John Wiley & Sons, New York.

Warren, G. J., 1980. "Radon in Vapor-Dominated Geothermal Reservoir," Engineer's Thesis, Stanford University, Stanford, CA.

Warren, G. J., and P. Kruger, 1979. "Radon Transients in Vapor-Dominated Geothermal Reservoirs," Report SPE-8000, Society of Petroleum Engineers of AIME.

Weast, R. C., and M. J. Astle, 1981. CRC Handbook of Chemistry and Physics. CRC Press, Boca Raton.

Yund, R. A., and T. F. Anderson, 1978. "The Effect of Fluid Pressure on Oxygen Isotope Exchange Between Feldspar and Water," Geachim. Cosmochim. Acta, 42, 235-239.